frontiers in Energy Research

ORIGINAL RESEARCH
published: 29 September 2021
doi: 10.3389/fenrg.2021.733842

Long-Term Global Solar Radiation Prediction in 25 Cities in Morocco Using the FFNN-BP Method

Brahim Belmahdi[1], Mohamed Louzazni[2], Mohamed Akour[1], Daniel Tudor Cotfas[3]*, Petru Adrian Cotfas[3] and Abdelmajid El Bouardi[1]*

[1]ETEE, Faculty of Sciences, Abdelmalek Essaadi University, Tetouan, Morocco, [2]Science Engineer Laboratory for Energy, National School of Applied Sciences, Chouaib Doukkali University, El Jadida, Morocco, [3]Department of Electronics and Computers, Transilvania University of Brasov, Brasov, Romania

This article presents different combinations of input parameters based on an intelligent technique, using neural networks to predict daily global solar radiation (GSR) for twenty-five Moroccan cities. The collected measured data are available for 365 days and 25 stations around Morocco. Different input parameters are used, such as clearness index K_T, day number, the length of the day, minimal temperature T_{min}, maximal temperature T_{max}, average temperature $T_{average}$, difference temperature ΔT, ratio temperature T-Ratio, average relative humidity RH, solar radiation at the top outside atmosphere TOA, average wind speed Ws, altitude, longitude, latitude, and solar declination. A different combination was employed to predict daily GSR for the considered locations in order to find the most adequate input parameter that can be used in the prediction procedure. Several statistical metrics are applied to evaluate the performance of the obtained results, such as coefficients of determination (R^2), mean absolute percentage error (MAPE), root mean square error (RMSE), normalized root mean square error (NRMSE), mean bias error (MBE), test statistic (TS), linear regression coefficients (the slope "a" and the constant "b"), and standard deviation (σ). It is found that the usage of input parameters gives highly accurate results in the artificial neural network (FFNN-BP) model, obtaining the lowest value of the statistical metrics. The results showed the best input of 25 locations, 12 inputs for Er-Rachidia, Marrakech, Medilt, Taza, Oujda, Nador, Tetouan, Tanger, Al-Auin, Dakhla, Settat, and Safi, seven inputs for Fes, Ifrane, Beni-Mellal, and Meknes, six inputs for Agadir and Rabat, five inputs for Sidi Ifni, Essaouira, Casablanca and Kenitra, four inputs for Ouarzazate, Lareche, and Al-Hoceima. In terms of accuracy, R^2 of the selected best inputs parameters varies between 0.9860% and 0.9920%, the range value of MBE (%) being from −0.1076% to −0.5931%, the RMSE between 0.1990 and 0.4580%, the range value of the NRMSE between 0.0355 and 0.8938, and the lowest value MAPE between 0.0019 and 0.0060%. This technique could be used to predict other parameters for locations where measurement instrumentation is unavailable or costly to obtain.

Keywords: artificial neural networks, solar prediction, daily global solar radiation, input parameters, statistical metrics

OPEN ACCESS

Edited by:
Enrico Maria Vitucci,
University of Bologna, Italy

Reviewed by:
Mustapha Elyaqouti,
Université Ibn Zohr, Morocco
Zineb Bounoua,
Sidi Mohamed Ben Abdellah University, Morocco

****Correspondence:***
Brahim Belmahdi
belmahdi.brahim@gmail.com
Daniel Tudor Cotfas
dtcotfas@unitbv.ro

Specialty section:
This article was submitted to Solar Energy, a section of the journal Frontiers in Energy Research

Received: *30 June 2021*
Accepted: *06 September 2021*
Published: *29 September 2021*

Citation:
Belmahdi B, Louzazni M, Akour M, Cotfas DT, Cotfas PA and El Bouardi A (2021) Long-Term Global Solar Radiation Prediction in 25 Cities in Morocco Using the FFNN-BP Method. Front. Energy Res. 9:733842. doi: 10.3389/fenrg.2021.733842

INTRODUCTION

In the last decade, energy demand has been growing internationally, with the rise in population growth and economic development. Thus, it becomes essential for the fulfillment of economic prosperity (Khan et al., 2016). Lately, the installed capacity of renewable energy has undergone a significant increase, reducing dangerous residues or the emissions of fossil fuel (Sayigh, 2017). All communities call for energy resources that fulfill essential needs, such as wellness, heating, eating, room comfort, accessibility, and connectivity and function as conceptual processes (Owusu and Asumadu-Sarkodie, 2016). Renewable energy, such as solar energy, wind energy, thermal energy, and hydroelectric energy, is widely accepted as the key tool for global sustainable economic development. Likewise, there seem to be two fundamental reasons behind the focus on sustainable energy: one is deforestation and global climate change, and the other is the possibility that fossil fuels will inevitably dry up and there will be no more oil, gas, and coal. That could also be said about nuclear energy since nuclear fuel stocks are not limitless (Kumar and Kumar, 2017).

Solar photovoltaic technology is gaining importance when it comes to addressing the issue of energy development for a number of reasons: the potential to transform solar radiation directly into power, the low cost, and the decreased pollution (Yu et al., 2017). In addition, the growth of the renewable energy industry thus produces new employment opportunities and contributes to improvement in air quality. However, the installation of solar electricity, such as photovoltaic (PV), concentrated solar power (CSP), or hybrid PV thermal installations, involves high-quality, decade-long time series of solar radiation data (Polo et al., 2020; Belmahdi and Bouardi, 2020). The long-term variability of solar radiation plays a major role in predicting the risk of the potential electricity production of a solar power plant being surpassed or unachieved and impacts the financial incentives that the project is expected to achieve. In this context, the information and behavior of solar radiation are very important for many sectors, such as agriculture, architect, design, and technology (Owusu and Asumadu-Sarkodie, 2016; Kaba et al., 2018). Generally, solar radiation energy has two components: terrestrial global and extraterrestrial solar energy (Rahimikhoob, 2010). The terrestrial solar radiation has direct (H_b) and diffuse (H_d) components. The sum of Hb*cosθ and H_d represents the global solar radiation (H_g); θ is the zenith angle. The measurement of energy use among houses, the development of heating ventilation and air-conditioning systems, and the use of solar energy need appropriate H_g data (Zhao et al., 2019; Liu et al., 2018). In particular, both direct and diffuse components are required to receive solar radiation on a slanted surface (Muneer et al., 2007). The best method for collecting data regarding solar radiation is focused on observations employing adequate equipment, but the measurements are rather time-consuming, the costs are high and the weather stations installation and management are demanding. For example, since 2019, there have been 17 cities in China where H_g and H_d, respectively, have been calculated (Feng et al., 2018) and 20 cities in Morocco where the solar radiation and other parameters have been collected through the project "proper.ma" (Aarich et al., 2018). In particular, there are challenges regarding long-term background measurement data, such as station changes and incomplete observations. However, the estimation and prediction of global solar radiation play a very important role. Several models have been developed in the literature to estimate and predict global solar radiation, which means it is difficult to choose the most accepted and efficient model for a particular use. In research areas, various solar radiation models have been developed for several years and they are categorized into three major models: empirical or analytical models, machine learning models, which use computational intelligence techniques, and satellite remote sensing models, as reported in Yang et al. (2020). Among all the presented models, all researchers have agreed on the importance of the results given by the Artificial Neural Network (ANN) (Kashyap et al., 2015; Al-Dahidi et al., 2019). The ANN was reported as the most used artificial intelligence technique for the prediction in several fields (Kashyap et al., 2015; Jiang, 2009). Celik and Muneer have presented and interpreted the relationship between solar radiation and other climatic parameters of the location selected (Celik and Muneer, 2013).

Generally, the ANN is the most used technique for the forecast or estimation of several things. For example, in Turkey, Sözen et al. (2004) have used the simple ANN to predict the solar radiation intensity using various parameters, such as latitude, longitude, altitude, month's number, average sunshine duration, and average temperature. The measurement data were collected from 17 different weather stations, where measurement data from 11 stations for training algorithm and other six measurement data are used for testing. In a different review, the same neural networks were used to predict the solar potential for 12 weather stations from Turkey. The performance of the results is validated by calculating the value MAPE = 6.78% and R^2 = 99.78% (Sözen et al., 2005). Sharifi et al. (2016) have implemented the feedforward neural network (FFNN) with four inputs in one hidden layer, one output layer, and Levenberg–Marquardt as a training algorithm. Using data from six stations, they have estimated the daily global radiation for two different countries, Iran (Tabriz and Urmia) and the United States (Grand Island, North Platte, Lincoln, and Scottsbluff). The used inputs are the daily mean clearness index (K_T), range temperature (ΔT), theoretical sunshine duration (N), and extraterrestrial radiation (R_a). The accuracy of the developed model was tested in terms of the average median absolute error (MAE = 7.4%), root mean square error (RMSE = 9.8%), and U95 = 27.35%. In Oman, Al-Alawi and Al-Hinai (1998) have used the FFNN with backpropagation training algorithm to predict global solar radiation. Eight input layers were implemented in ANN, namely, location, month, mean pressure, temperature, vapor pressure, relative humidity, wind speed, and sunshine duration. The accuracy of the results was tested by Mean Absolute Percentage Error percentage (MAPE) with 7.3%. In Morocco, Bounoua et al. (2021) have used the neural network method, 22 empirical models, and tree-based ensemble methods to estimate the daily GSR in five studies locations. In terms of accuracy, the proposed methods were evaluated using R^2, NRMSE, and NMAE.

As a result, the random forest method outperforms the other techniques with the highest value of R^2 and lowest value of NRMSE and NMAE.

In China, Lam et al. (2008) have applied the multi-layer FNN (MLFFNN) to estimate the daily global solar radiation using measured sunshine duration for 40 cities covering nine major thermal climatic zones and sub-zones in China. Six input layers were used: latitude, longitude, altitude, day number, temperature, and sunshine ratio. The quality of the estimated results was verified by the calculation of the statistical performance. The MBE values vary between 16.9% underestimation to 18.6% overestimation, and RMSE values vary in the range from 9.1 to 20.5%. In another paper, in Zimbabwe, Chiteka and Enweremadu (2016) have implemented the FFANN to predict the global horizontal irradiation (GHI) using geographical and meteorological data for 20 locations. 12 locations were used in the ANN training algorithm and other data from eight locations were included in the simulation with seven inputs, namely, altitude, latitude, longitude, relative humidity, pressure, clearness index, and average ambient temperature, one hidden layer, and one input layer. The quality of the predicted results is carried out by calculating the performance indexes such as coefficient of determination R^2, RMSE, MAE, and MAPE with the following values 99.894%, 0.223 Kwh/m^2, 0.17 Kwh/m^2, and 2.56%, respectively.

In Italy, Alsina et al. (2016) have applied the FFNN to forecast the monthly average daily global solar radiation (MDGSR) for 45 different locations. Different input parameters were taken into account, such as meteorological and geographical coordinates. The measurement data from 17 destinations have been used for training, whereas other collected data have been for testing the ANN. The most appropriate input parameters are the automatic relevance determination (ARD) and Bayesian method. The appropriate architecture of the suggested ANNs contained seven input parameters, i.e., TOA, duration of day, number of rainy days, average temperature, latitude, and altitude. The quality and accuracy of the model were tested and validated by calculating the MPE, which varied from 1.67 to 4.25%, NRMSE 1.01–1.65%, and MPBE from -0.20 to 0.03%.

In Spain, Hontoria et al. (2005) have implemented MLP to predict the solar radiation map. This study collected the measurement data from seven different lections. The aim was to generate a time series of hourly solar radiation using specific characteristics, such as temperature and latitude. In other articles in Egypt, Elminir et al. (2007) have proposed two kinds of ANN to predict the hourly and daily diffuse solar radiation using the Multi-Layer Perceptron (MLP) with backpropagation training algorithm. A different type of parameters is selected for the input of the ANN, such as hour, day, month, year, hourly global radiation, and hourly extraterrestrial solar radiation, and the output was the hourly diffuse radiation. On the other hand, three different inputs were considered input layers of the neural network, namely, global solar radiation, extraterrestrial solar radiation, and sunshine ratio for predicting daily diffuse solar radiation. The results of the study using the ANN model were compared with those of the linear regression models and were used for the models on the hourly and daily scales. In both, the ANN results are more accurate in predicting diffuse solar radiation. In India, Alam et al. (2006) have implemented the feedforward backpropagation network (FFBPN) to predict the solar radiation, and the selected inputs were the latitude, longitude, attitude, months of years, rainfall ration, mean duration of sunshine per hour, and ratio of relative humidity. The performance of the predicted results was calculated using the RMSE = 1.65% and MBE = 2.79%. Mehleri et al. (2010a) have used the neural network radial basis function (NNRBF) to predict solar radiation on the inclined surface by applying the optimum angle for a specific site. The NNRBF used the tilted angle and orientation as input and fuzzy logic for the training algorithm. The accuracy of the results was validated by calculating the coefficient of determining R^2 = 99.99%. In another study, the same researchers have used the RBFNN to predict the solar radiation on inclined surfaces and total solar irradiance on a horizontal surface. The extraterrestrial radiation, solar zenith angle, and solar incidence angle on a tilted plane are considered input data for Athens, Greece. The performance of the results is validated by the R^2 = 96%. On the other hand, three different ANN models were developed in Ajaccio, France, by Notton et al. (2012) to predict the hourly solar radiation on an inclined surface for Mediterranean locations. Different parameters were chosen as inputs: the declination angle, hour, zenith angle, hourly extraterrestrial horizontal irradiation, and hourly global irradiation. The first and second models of ANN predicted the hourly global solar radiation for two angles 45° and 60° and the third model for angles 45° and 90°. The obtained results showed that R^2 in the three models is equal to 99.79%, 99.82%, and 99.70%, respectively. Moreover, Celik and Muneer (2013), in Iskenderun, Turkey, have adopted a model using the generalized regression neural networks (GRNN) to estimate the solar radiation on an inclined surface. Three parameters are used here as input data: global solar irradiation on a horizontal surface, declination, and hour angles. The accuracy of the results is validated by R^2 for evaluated values as 98.7% at 14.9 kwh/m^2.

In Algeria, a simplified hybrid model was developed by Gairaa et al. (2016) using the linear autoregressive moving average (ARMA) model combined with ANN to predict the daily global solar irradiation using measurement data from two locations. The input of the proposed model is the clearness index, while the output is the daily global solar radiation. The calculated performance error metrics were MPE = 18.1 and 2.7% for the first location and MAPE = 7.26 and 1.39% for the second locations. In another publication in the same country, Mellit et al. (2005) have combined the ANN with Markov transition matrix (MTM) to predict daily global solar radiation. The output data were the daily global solar radiation and the geographical coordinates, such as latitude, longitude, and altitude, were the input data of the neural network layer. The performance of the hybrid ANN-MTM model was calculated to verify the accuracy of the predicted results and was given as RMSE = 8%, R^2 varying in the range of [0.9 0.92] (Belmahdi et al., 2020a).

According to the cited references above, there are various applications of the ANNs to predict/estimate or forecast global solar radiation in different locations and angles. Here, we can cite the predicted solar radiation at the horizontal and tilted surface:

TABLE 1 | Current parameters adopted in the literature to predict and estimate global solar radiation.

Parameters		References
Geographical coordinate	Latitude	Al-Alawi and Al-Hinai (1998); Sözen et al. (2004); Mellit et al. (2005); Sözen et al. (2005); Alam et al. (2006); Lam et al. (2008); Notton et al. (2012); Khatib et al. (2012); Chiteka and Enweremadu (2016); Siva Krishna Rao et al. (2018)
	Longitude	Al-Alawi and Al-Hinai (1998); Sözen et al. (2004); Sözen et al. (2005); Alam et al. (2006); Lam et al. (2008); Chiteka and Enweremadu (2016); Gairaa et al. (2016); Siva Krishna Rao et al. (2018)
	Altitude	
Climatological parameters	Pressure	Al-Alawi and Al-Hinai (1998); Celik and Muneer (2013); Chiteka and Enweremadu (2016)
	Clearness index	Hontoria et al. (2005); Mellit et al. (2005); Elminir et al. (2007); Lam et al. (2008); (Mehleri et al., 2010b); Gairaa et al. (2016)
	Sunshine duration	Al-Alawi and Al-Hinai (1998); Sözen et al. (2004); Sözen et al. (2005); Alam et al. (2006); Lam et al. (2008); Khatib et al. (2012); Celik and Muneer (2013); Siva Krishna Rao et al. (2018)
	Temperature	Sözen et al. (2004); Sözen et al. (2005); Celik and Muneer (2013); Chiteka and Enweremadu (2016); Sharifi et al. (2016)
	TAO	Mellit et al. (2005); Lam et al. (2008); Sharifi et al. (2016)
	The length of the day	Al-Alawi and Al-Hinai (1998); Hontoria et al. (2005); Khatib et al. (2012); Celik and Muneer (2013); Chiteka and Enweremadu (2016)
	Atmosphere pressure	Al-Alawi and Al-Hinai, (1998)
	Relative humidity	Alam et al. (2006); Lam et al. (2008); Li et al. (2015); Chiteka and Enweremadu (2016); Sharifi et al. (2016); Siva Krishna Rao et al. (2018)

TABLE 3 | Climatological and geographical parameters.

Input's vector	Input parameters	Unit
x_1	Clearness index (K_t)	—
x_2	Day number	—
x_3	The length of the day	hours
x_4	T_{min}	°C
x_5	T_{max}	°C
x_6	$T_{avearge}$	°C
x_7	Delta-T (ΔT)	°C
x_8	T-Ratio (T_{Ratio})	°C
x_9	Average humidity (R_h)	%
x_{10}	TOA radiation	KWh/m^2
x_{11}	Average of wind speed (W_s)	m/s
x_{12}	Altitude (Alt.)	degrees
x_{13}	Longitude (Long.)	degrees
x_{14}	Attitude (Att.)	M
x_{15}	Solar declination (δ)	degrees
	Output parameter	Unit
y_1	Daily global solar radiation	KWh/m^2

different meteorological and geographical coordinates have been considered by multiple authors, e.g., latitude, longitude, altitude, wind speed, clearness index, air temperature, sunshine duration, top of atmosphere (TOA) radiation, and rainfall. **Table 1** illustrates the most often used input parameters in ANNs categorized into geographic coordinates and climatologic parameters.

In this context, this research is specifically intended to suggest an intelligent paradigm for evaluating and identifying the appropriate input possibilities that can include the highest potential correlations and simplifications with this proposed study, relying on the fact that predictions of solar radiation can be enhanced with ANN models using different input parameters, e.g., location, weather information, and neighboring stations, and other input parameters. According to Yadav and Chandel (2014), the solar radiation predicted by ANNs is correct compared to that by empirical models. Moreover, the ANNs have different single layers, FFBP, or combined with other techniques, and the second is the most widely used in solar radiation. It has forward relations between inputs and outputs across various hidden layers. The main contribution of this study is to investigate and predict daily global solar radiation based on various combination inputs for 25 cities in Morocco. In fact, relying on the FFNN-BP methods, the suggested method would promote correlations among all feasible input configurations in order to select the best input parameters that can provide better results with the lowest values of statistical indicator performance, which present a good approximation with measured data.

METEOROLOGICAL CLIMATE IN MOROCCO

Morocco has a wonderful opportunity to access sustainable energy options that will address two of the burning issues in the country: electricity availability and global warming challenges. Generally, Morocco has a powerful capacity in sustainable resources, primarily solar and wind, with the potential level of generation varying from 20,000 to 25,000 MW (Šimelytė et al., 2020; Belmahdi and El Bouardi, 2020). On a world wide scale, Morocco holds the sixth rank for solar and the seventh place for wind. The average daily value of solar radiation intensity in Morocco is close to 5.80 kWh/m^2/day. Meanwhile, Morocco has many sustainable energy programs being implemented and one of the biggest solar energy programs in the world is expected to cost $7.8 billion. This innovative and practical national effort focuses on creating a potential of 2,000 MW by 2020. This generation capacity constitutes 38% of mounted energy by the end of 2008 and 14% of electrical power by 2020.

In this context, it is necessary to analyze and predict the solar radiation behavior for all considered locations in Morocco. The solar radiation depends on and is affected by various parameters, such as altitude and longitude. However, this research aims to present data for 25 various regions with different climatic conditions and geographical features prevalent in all parts of Morocco. The locations are divided to six zones characterized by

TABLE 2 | Average data of 25 locations and geographical coordinates.

Zone	Site	TOA (KWh/m^2/day)	GSR (KWh/m^2/day)	Kt	T_{mean}(°C)	T_{max}(°C)	T_{min}(°C)	ΔT(°C)	T_{ratio}(°C)	R_h(%)	W_s(m/s)	δ	Long(degree)	Lat(degree)	Alt(degree)
Z1	Kenitra	5,413	8,143	0,658	17,587	22,4	13,3	8,9	1,6573	80,792	2,675	12,377	−6,6	34,3	14
	Casablanca	5,139	8,188	0,625	18,367	21,8	15,2	6	1,369	80,917	1,913	12,435	−7,667	33,567	55
	Rabat	5,453	8,130	0,650	17,475	22,2	13,3	8,9	1,6364	81,333	2,671	12,387	−6,767	34,05	75
	Safi	5,615	8,340	0,668	19,283	24,7	14,5	11	1,7342	64,042	2,238	12,519	−9,233	32,283	45
	Agadir	5,396	8,593	0,648	19,65	25,2	14,4	11,4	1,7965	67,75	2,988	12,532	−9,567	30,383	23
	Essaouira	5,591	8,446	0,659	19,979	25,4	14,8	10,4	1,6567	61,5	3,750	12,545	−9,783	31,517	8
	Settat	5,471	8,598	0,651	19,654	25,1	14,2	11,4	1,8027	67,417	2,992	12,524	−9,41	30,33	74
	Dakhla	5,700	9,290	0,606	20,271	23,3	17,5	5,7	1,3146	74,417	6,829	12,771	−15,867	23,7	10
	El-Aiun	5,737	8,936	0,650	20,7	24,9	16,8	8,2	1,4835	66,833	6,154	12,695	−13,21	27,16	64
	Sidi Ifni	5,042	8,734	0,620	19,358	21,4	17,4	4	1,2353	72,542	2,892	12,561	−10,18	29,36	66
Z2	Tanger	5,392	7,991	0,681	17,429	21,8	13,3	8,6	1,5878	73,542	4,708	12,338	−5,9	35,733	21
	Tetouan	4,909	8,009	0,653	18,671	22,4	15,5	7,1	1,4233	70,083	4,263	12,306	−5,33	35,58	10
	Al-Hoceima	5,160	8,038	0,660	17,546	21,2	14,3	7,3	1,5	72,458	2,204	12,222	−3,85	35,18	14
	Larache	5,488	8,038	0,680	18,529	22,4	14,8	7,6	1,4844	74,417	2,475	12,351	−6,13	35,18	49
	Nador	5,001	8,040	0,650	18,046	23,1	13,3	10,1	1,7219	71,792	2,771	12,168	−2,91	35,15	16
Z3	Oujda	5,169	8,063	0,686	16,754	23,1	10,7	12,6	2,0625	63,125	3,338	12,112	−1,933	34,783	470
	Taza	5,475	8,119	0,681	17,917	23	13,1	10,4	1,717	61,75	1,454	12,23	−4	34,217	510
	Meknes	5,371	8,143	0,664	16,946	22,8	11,8	11,5	1,9172	63,625	2,683	12,317	−5,533	33,883	549
	Beni-Mellal	5,405	8,315	0,670	18,692	25,6	12,7	13,5	1,9648	58,417	1,675	12,364	−6,4	32,36	468
	Ifrane	5,269	8,184	0,688	14,246	20,3	9,1	12	2,0256	50,292	2,783	12,297	−5,167	33,5	1665
	Fes	5,129	8,137	0,669	16,7	23,3	10,6	12,7	2,1	61,708	3,054	12,286	−4,983	33,933	579
Z4	Medilt	5,690	8,272	0,718	14,546	20,7	9,4	11,2	2,0467	51,292	2,283	12,272	−4,733	32,683	1515
Z5	Marrakech	5,590	8,411	0,685	20,117	26,2	14,8	12,3	1,8086	50,667	2,333	12,453	−8,033	31,617	466
Z6	Ouarzazate	6,214	8,489	0,732	19,729	26,5	13,3	12,8	1,8721	29,292	2,667	12,391	−6,9	30,933	1140
	Er-Rachidia	6,060	8,352	0,729	20,108	25,9	14,8	11	1,7267	38,042	2,288	12,253	-4,4	31,93	1045

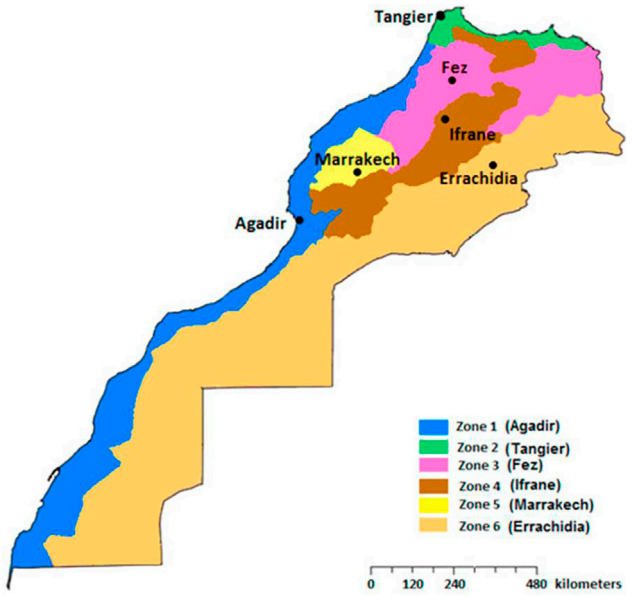

FIGURE 1 | Climatic zoning of Morocco [adapted from National Agency for the Development of Renewable Energy and Energy Efficiency (ADEREE)].

the following parameters: the latitude varies from 23,7° to 35,733° and the longitude varies from −15,867° to −2,91°, whereas the altitude varies from 8 to 1665 m. **Table 2** presents the average data of the 25 locations and geographical coordinates.

Morocco's climate is both Mediterranean and Atlantic, varying from dry to hot season combined with a cool and rainy season. The influence of the sea modulates temperature differences, tempers seasons, and raises the humidity of the environment. Bouhal et al. (2018) and Allouhi et al. (2015) have presented Morocco in six different zones adopted according to the Moroccan Agency for Renewable Energies and Energy Efficiency for concentrated solar power use, as presented in **Figure 1**.

ARTIFICIAL NEURAL NETWORKS

The application of the ANN has gained growing interest in recent years to address several real-world problems. It has been widely used to address several difficult issues where conventional issue approaches either struggled or proved to be ineffective or unsuccessful (Kamruzzaman et al., 2006). ANN is widely used in various fields, such as solar energy, wind (Tagliaferri et al., 2015), electricity (Khwaja et al., 2020), mechanics (Sterjovski et al., 2005), astrophysics (George and Huerta, 2018), partial differential equations (ShekariBeidokhti and Malek, 2009), polymers (Amirian et al., 2018; Kaplan, 2018) or in optimization, control, modeling, and solar radiation forecasting (Belmahdi et al., 2020b).

The neural network structure schematically mimics a human brain network, containing thousands of neurons that are specifically linked to each other. Throughout the biological context, the neuron receives a variety of inputs from other inputs and integrates them in some direction. Every other neuron is responsible for performing basic computation only. Meanwhile, the effects of the procedure are usually nonlinear, and the output is the final product. In either scenario, the configuration of an artificial neuron is easier than a biological neuron (Pacheco-Vega et al., 2001; Kamruzzaman et al., 2006). In addition, the complex architecture of the biological neural networks translates the area of the ANN. Feedforward ANNs (FF-ANNs) are formed through recurring ANNs and repeated ANNs, like feedback loops (Yalçın et al., 2020). The FNNs are those ANNs with only single-way interactions between their neurons (Bebis and Georgiopoulos, 1994).

The ANNs are considered in the research area as data-driven models (Chakraborty et al., 1992; Boland et al., 2001; Durna and Şahin, 2020) and consist of two layers considered as input and output: the first is to receive the data, while the second is the hidden layer displaying the simulated results (Yalcintas and Akkurt, 2005). The hidden layer also learns, memorizes, and creates relationships between output and input data (Moreno et al., 2011). Generally, the ANN training mechanism is related by changing the weights of every connection. The connection between the neural network layer may be investigated by weighting coefficients (w) and bias (B) for increasing processor and activation function, such that the network tries to generate the optimal performance close to the real performance, as illustrated in **Figure 2** (Yilmaz and Özer, 2009).

Following the initial training phase, performance can be viewed as network integration and it is important to follow a backpropagation (BP) appropriate learning algorithm to minimize the errors during the simulation (Riahi-Madvar

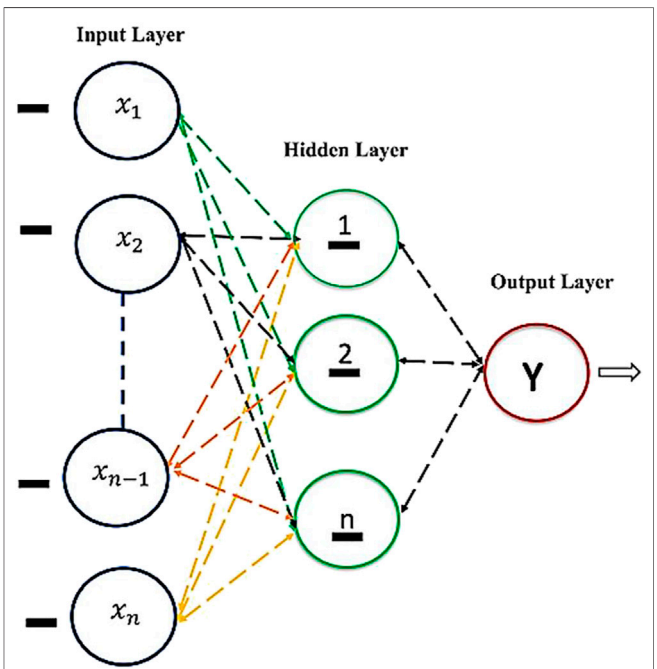

FIGURE 2 | Structure architecture of an MLP neural network.

et al., 2011). The main objective of using the BP algorithm method is to reduce the size of a network error. The BP based on gradient descent can be calculated by the following equation (Al-Alawi and Al-Hinai, 1998):

$$e = 0.5 \sum_{k=1}^{N} (O_k - t_k)^2, \quad (1)$$

where N represents the number of processors, O_k is the output result in the K-th processor, and t_k denotes the target values.

In the BP algorithm, there are two steps of the training process: one to reproduce the input signal across the network and the other to follow the output by adjusting the weights in the network. Those are the error indicators that are back-spread to the hidden layer(s) throughout the network operation. The output layer error is being used as the basis for correcting the relation weights between both the origin and the hidden layers (Khare and Nagendra, 2007). The modification of both the relation weights between the input and the hidden layers and the corresponding recalculation of the output values will once more be a small sensitivity point since the iterative procedure is carried out before the error decreases. The BP training algorithm begins by copying and pasting the simulation data collection to the network, and the simulation data collection is made up of input and output vectors. Once certain vectors are dynamically introduced to the neural network, the following equations are implemented:

$$Z_j = \sum_{ij} W_{ij}\left(X_i + b_j\right), \quad i = 1, 2, \ldots . n; \; j = 1, 2, \ldots . h, \quad (2)$$

where Z_j represents the input to the j-th hidden layer neuron, X_i is the numerical value of the i-th input vector, W_{ij} is the weight of the i-th input layer neuron to the j-th hidden layer neuron, n and h represent the number of the input and hidden layer neurons, respectively, and b_j is the bias value for the j-th hidden layer neuron.

The function in the output of the hidden layer using the sigmoid function is determined as follows:

$$h_j = f\left(Z_j\right) = \frac{1}{1 + e^{-Z_j}}, \quad j = 1, 2, \ldots . h, \quad (3)$$

with f representing the transfer function for the hidden layer.

In addition, the performance of the network will not be equivalent to the target performance during the training process. Consequently, the output error is measured as the difference between the output and the desired input of the network. If the output error does not reach the acceptable level, the network adjusts the interaction weights according to the output error significance; instead, the training data are re-entered to the network and the output of the network is determined (Battiti, 1992). The training process will proceed until the network reaches the optimal degree of tolerance. If the error value is below the tolerance range, the network should become a "qualified" network (Haykin, 1988). Then, BP algorithm is outlined in the following seven steps:

1) Initialize the network weights.
2) Analyze the first input vector from the training data and present it to the network.
3) Propagate the input vector across the network to get an output.
4) Determine the error by calculating the difference between the output and the input.
5) The error will be propagated back to the network.
6) Change the weights to eliminate the cumulative error.
7) Repeat steps (2) to (7) for the next input vector until those errors are satisfactorily minimal.

The BP algorithm includes two adaptive variables, a learning rate η and a moment term μ, which will improve the training method by eliminating the local minimum. η identifies the measure provided along the iterative gradient of descent learning method, and μ is used to encourage the gradient descent operation because it is trapped to a local minimum. **Figure 3** depicts the FFNN with a backpropagation algorithm structure.

The definition "feedforward" implies that a neuron association occurs either from the neurons in the input layer to other neurons in the hidden layer or from the neurons in the hidden layer to the neurons in the output layer, and the neurons inside the layer are not interconnected.

PREDICTION MODEL ARCHITECTURE

The described FFNN-BP model is implemented to predict the daily global solar radiation in 25 different Moroccan cities (El Mghouchi et al., 2016; El Mghouchi et al., 2019). The FFNN-BP model operates with the monitoring of the learning approach and the Levenberg–Marquardt training algorithm, as illustrated by Al-Alawi and Al-Hinai (1998). The training step is the most important and essential aspect of the neural network. The training algorithm is used to adopt and fix the ANNs by training and changing the weight to find the accurate output (Sözen et al., 2005). The used structure of the FFNN-BP model is shown in **Figure 4**.

The data collected across different locations were separated into "training dataset" and "validation dataset" and were rendered taking into account weather conditions. The FFNN-BP model used 15 input data organized in the following vector as input parameters:

$$X = [x_1 \; x_2 \cdots\cdots x_{15}]. \quad (4)$$

Table 3 presents the vector X input variable of the network. While the ten neurons are used in one hidden layer, they are followed by one output layer. At the first step, we used the data collected from station 1 for 1 year for neural network training, which offered 365 pairs of input and outputs for training when the neural network started the training process. It is noticed that some error function was well-defined until the training process described in **Eq. 1** approaches a minimum value. After this step, the predicted model was used for testing, where the data from a similar station are used.

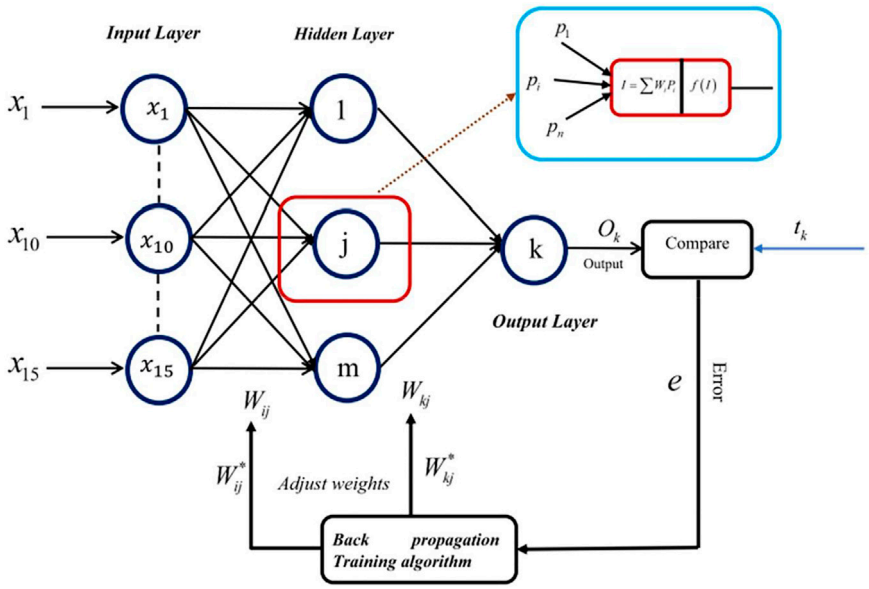

FIGURE 3 | Structure of FFNN with backpropagation algorithm.

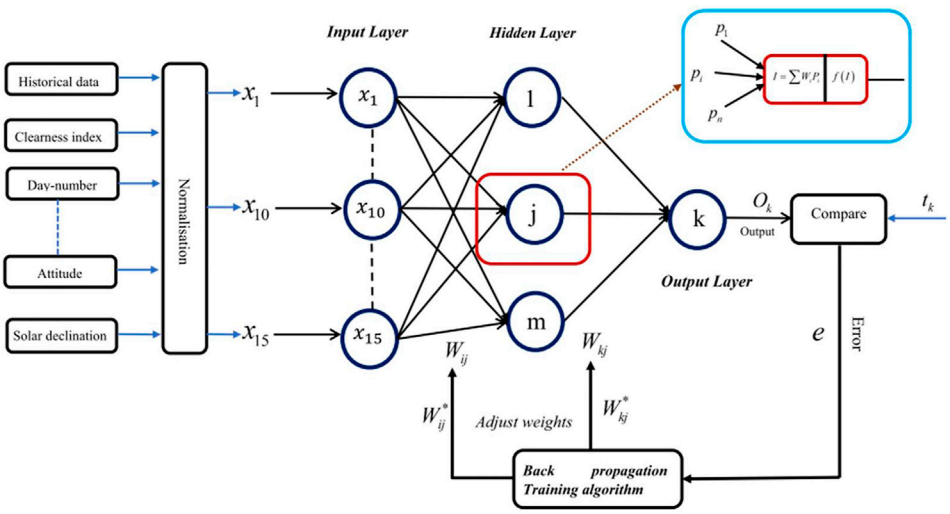

FIGURE 4 | Structure of used FFNN-BP model.

Some of the 15 input parameters used and computed are as follows: sun declination δ, the length of the day D_{length}, TOA, and K_t. They are calculated using the given formulas in the literature by the following equations (Belmahdi et al., 2020b; Rajendran and Smith, 2016):

$$\delta = 23.45 \sin[0.986(N + 284)], \tag{5}$$

$$D_{length} = 24\left[1 - \cos^{-1}[\tan(\delta).\tan(\lambda)./\pi]\right], \tag{6}$$

$$TOA = \int^{day} I_0 E_0 \sin(h) dt, \tag{7}$$

$$Kt = \frac{DGSR}{TOA}, \tag{8}$$

where N represents the Julian day, λ is the longitude, I_0 is the solar constant, h is the solar elevation, and E_0 is the correction of the Earth–Sun distance.

In order to test the quality and the performance of the used FFNN-BP model, we propose to calculate and compare several errors metrics. These error metrics are widely used in the research area to test the validity and accuracy of the results, like in photovoltaics (Al-Dahidi et al., 2019; Louzazni et al., 2020). In this article, the error metrics are organized into two categories, as given by Gueymard (2014). The details about the error metrics are mentioned in the following equations:

1) Indicators of dispersion

Mean bias error (MBE)

$$MBE = \frac{1}{K}\sum_{i=1}^{K}\left(G_{forcast,i} - G_{\exp,i}\right). \quad (9)$$

Root mean square error (RMSE)

$$RMSE = \sqrt{\frac{1}{K}\sum_{i=1}^{K}\left(G_{forcast,i} - G_{\exp,i}\right)}. \quad (10)$$

Normalized root mean square error (NRMSE)

$$NRMSE = \sqrt{\frac{1}{K}\sum_{i=1}^{K}\left(G_{forcast,i} - G_{\exp,i}\right)}/\frac{1}{K}\sum_{i=1}^{K}G_{\exp,i}. \quad (11)$$

Mean absolute percentage error (MAPE)

$$MAPE = \frac{100}{K}\sum_{i=1}^{K}\left|\frac{G_{forcast,i} - G_{\exp,i}}{G_{\exp,i}}\right|. \quad (12)$$

2. Indicators of overall performance

Coefficient of Determination R^2

$$R = 1 - \frac{\sum_{i=1}^{K}\left(G_{forcast,i} - G_{\exp,i}\right)^2}{\sum_{i=1}^{K}\left(G_{forcast,i} - \overline{G}_{\exp,i}\right)^2}. \quad (13)$$

The linear regression coefficients are as follows:

$$Y = aG + b, \quad (14)$$

$$a = \overline{G_{forecast}G_{\exp}} - \frac{\overline{G_{\exp}G_{forecast}}}{\overline{G^2}_{\exp} - \overline{G}^2_{\exp}}, \quad (15)$$

$$b = \overline{G}_{forecast} - a\overline{G}_{\exp}, \quad (16)$$

where K is the total number of observations, $G_{forecast}$ and $G_{\exp}$ are the forecasted and measured values of daily global solar radiation (daily GSR), respectively, $\overline{G}_{forecast}$ and $\overline{G}_{\exp}$ represent the average of forecasted and measured values of daily solar radiation.

It should be mentioned that the smaller values of MBE, RMSE, NRMSE, and MAPE show more accuracy than the predicted values and an ideal case is zero. All these statistical indicators or error metrics have the added advantage of indicating whether the estimated values are statistically significant or not at a particular confidence level. The error formulations of MBE and RMSE provide quantitative measures that have the same physical units as the dependent variable. The NRMSE and R^2 are dimensionless and the MAPE provides quantitative measures in percentage.

RESULT ANALYSIS AND DISCUSSION

The feedforward backpropagation was used to predict daily global solar radiation using the neural network toolbox of MATLAB 2012 software. Particularly, other authors have pointed out a multi-step prediction model: collecting data, creating a network, configuring the network, modeling, initializing weight and biases, training the network, and validating and using the network. One of the most important issues in this article is how the model was selected to perform a series of solar radiation values transversely.

Firstly, the Quantile-Quantile (Q-Q) graph is used to evaluate the goodness of fit for the used FFNN-BP model and recognize the performance models of global solar radiation values. For daily GSR, the Q-Q graph, presented in **Figure 5**, shows the comparison of simulated daily global solar radiation generated by ANN model. Against the measured data, an overestimation and an underestimation of solar radiation for 25 locations appear. Although the graphs of all study places accurately simulated the global solar radiation, this result indicates that the FFNN-BP model is accurate to be employed in all study locations of Morocco.

In the following prediction, all inputs parameters variables are applied to train and validate the FFNN-BP model. These input parameters data are divided into three categories, 80% for training, 10% for testing, and 10% for validation, to choose the most suitable input scenario of the models. It is noted that Rao et al. (Siva Krishna Rao et al., 2018) and Huang et al. (Huang and Shih, 2003) have explained the multiple steps phases of the ANN architecture. We adopt in this article the methodology used in (Huang and Shih, 2003), adopted as the first step (training). It is useful to start with a minimum number of neurons in the hidden layer of artificial Intelligent (AI). The number of these neurons will continually increase and retraining of the AI is continued, until the significant training of ANN is achieved and a suitable number is selected, as indicated in **Table 4**. After several trials, the ten neurons are considered a hidden layer (Yadav et al., 2014; Mba et al., 2016); the standard criteria for choosing among of ANN models are Mean Square Error (MSE). Moreover, various experimental parameters data used in the proposed models are presented in **Table 4**.

Binomial coefficient or combination can be estimated using the following mathematical expression:

$$C = \sum_{p=1}^{m} C_m^p = \sum_{p=1}^{m}\frac{m!}{(m-p)!p!}, \quad (17)$$

where C is the number of all combinations and m is the total number of inputs.

Hence, 32,767 combinations were found. All results should be compared for selecting the optimum inputs parameters that can predict the output parameters. After several trials, we found a total of 125 considered an adequate combination to predict the daily global solar radiation of all considered study locations in Morocco. In addition, the ANN process started with the selection of input combinations. For a good fitting, we train the network more before predicting the output results. In another study, Silva et al. (Siva Krishna Rao et al., 2018) have developed six ANNs using several input data with 32 possible combinations of inputs. The input parameters are as follows: theoretical sunshine hours (S_0), sunshine hours (S), extraterrestrial radiation (H_o), daily minimum and maximum of temperature, difference of daily maximum temperature, and difference of daily minimum

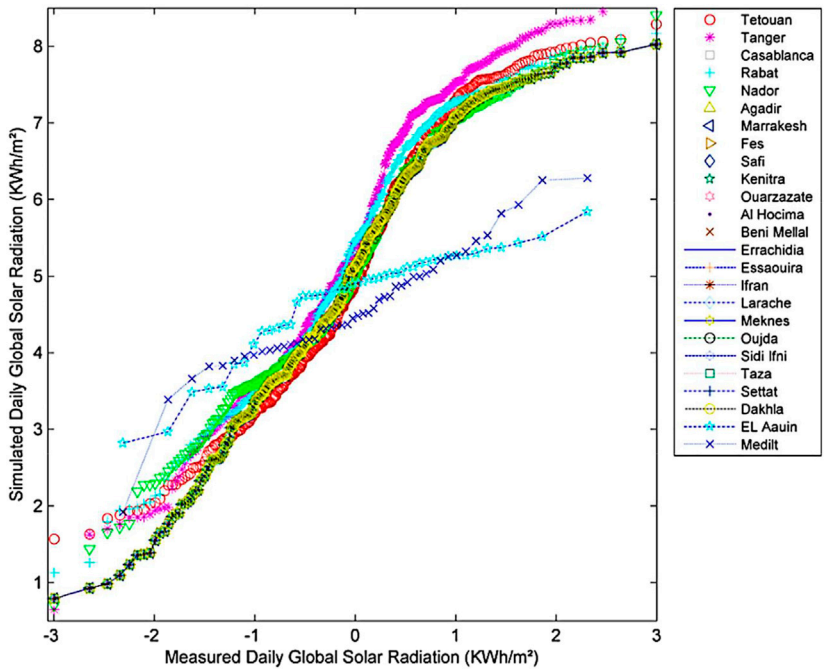

FIGURE 5 | Q-Q plot of measured and simulated daily global solar radiation generated by FFNN-BP model for 25 Moroccan locations.

TABLE 4 | ANN models with different input combinations.

Number of inputs	Combination of inputs
x_1	K_t
x_2	K_t, TOA
x_3	K_t, TOA, T_{max}
x_4	$K_t, TOA, T_{max}, T_{ratio}$
x_5	$K_t, TOA, T_{max}, T_{ratio}, \Delta T$
x_6	$K_t, TOA, T_{max}, T_{ratio}, \Delta T, T_{Average}$
x_7	$K_t, TOA, T_{max}, T_{ratio}, \Delta T, T_{Average}, T_{min}$
x_8	$K_t, TOA, T_{max}, T_{ratio}, \Delta T, T_{Average}, T_{min}, Long$
x_9	$K_t, TOA, T_{max}, T_{ratio}, \Delta T, T_{Average}, T_{min}, Long, Alt$
x_{10}	$K_t, TOA, T_{max}, T_{ratio}, \Delta T, T_{Average}, T_{min}, Long, Alt, Lat$
x_{11}	$K_t, TOA, T_{max}, T_{ratio}, \Delta T, T_{Average}, T_{min}, Long, Alt, Lat, \delta$
x_{12}	$K_t, TOA, T_{max}, T_{ratio}, \Delta T, T_{Average}, T_{min}, Alt, Long, Lat, \delta, D_{length}$
x_{13}	$K_t, TOA, T_{max}, T_{ratio}, \Delta T, T_{Average}, T_{min}, Alt, Long, Lat, \delta, D_{length}, D_{number}$
x_{14}	$K_t, TOA, T_{max}, T_{ratio}, \Delta T, T_{Average}, T_{min}, Alt, Long, Lat, \delta, D_{length}, D_{number}, W_s$
x_{15}	$K_t, TOA, T_{max}, T_{ratio}, \Delta T, T_{Average}, T_{min}, Alt, Long, Lat, \delta, D_{length}, D_{number}, W_s, R_h$

temperature. The methodology adopted in this study is presented in **Figure 6**.

Furthermore, the selected input parameters are tested using the linear relationship with measured daily global solar radiation (**Table A1**). The expression of the linear relationship is given in the following equation:

$$M_{DGSR} = b_0 + b_1 K_t + b_2 TOA + b_3 T_{\max} + \cdots\cdots b_{15} R_{rh}. \quad (18)$$

For a more specific analysis, the Taylor diagram is used as a comparative method between measured and predicted values. The following statistical error metrics, correlation coefficient (R^2), root mean square error (RMSE), and standard deviation (σ), were combined in a polar diagram (two-dimensional). In order to compare the performance of the most suitable input-output parameters of all considered locations, all graphs based on the statistical error metrics are presented in **Figure 7**. The illustrated figures present the lowest value of RMSE and standard deviation (σ). The highest value of R^2 represents the accuracy relationship between measured and predicted values.

The FFNN-BP model performance is presented with the top five selected input parameters of all twenty-five cities and is shown in **Table 5**.

The FFNN-BP models, based on different input parameters, have the capability of finding relationships between the

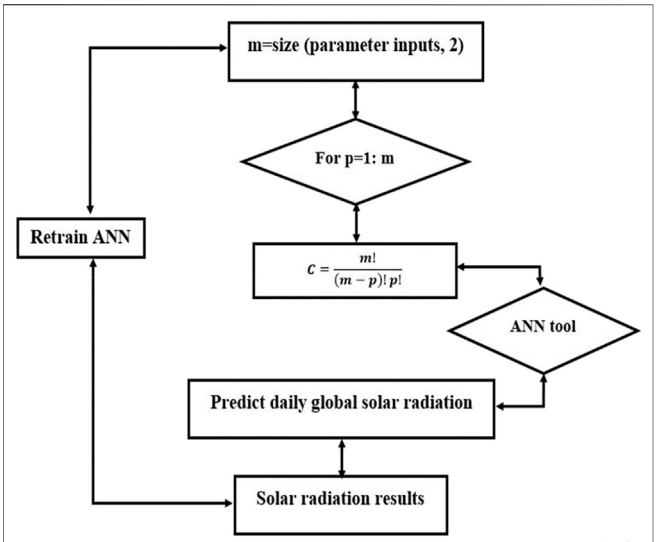

FIGURE 6 | The proposed methodology adopted.

variation of each input parameter and the variation of the output parameters. This variation is related to the daily GSR using the proposed method. All statistical metrics performance of the five best inputs parameters indicates that the ANN performs better. Based on R^2 results, all five best inputs of six zones have shown high prediction accuracy. Best performance in the first zone is obtained by the lowest value of MBE, RMSE, NRMSE, MAPE, TS, and σ, respectively. It is reported that the twelve input parameters are the most selected of the following cities: Safi, Settat, Dakhla, and Al-Auin; however, the inputs D_{number}, W_s, and R_h are based on MBE, RMSE, NMRSE, MAPE, TS and K_t, TOA, T_{max}, T_{ratio}, ΔT, $T_{average}$, T_{min}, Alt, Long, δ, and D_{length}, which have shown excellent estimation. Rabat and Agadir present six input parameters for Kenitra, Casablanca, Essaouira, and Sidi Ifni and five input parameters were selected as the most suitable. For the second zone, the selected input parameters are twelve for Tanger, Tetouan, and Nador, whereas four input parameters are considered as the best input parameters of Al-Hoceima and Laareche. For the third zone, twelve parameters were found for Oujda and Taza as the best input data. For the other locations, seven parameters are found as the best inputs. One site in the fourth and five zones shows that the twelve parameters are the best inputs. The other zones present two best inputs. For Ouarzazate, there are four parameters and for Er-Rachidia, there are twelve parameters. According to the results, it is suitable to obtain the founded input parameters as basic information for developing new solar radiation based on different meteorological data and parameters coordinates.

Figure 8 presents the scattered plot of daily GSR values predicted by the proposed model of the best-found parameters (twelve, four to seven inputs) with measured daily GSR values. The figures show that the lowest values of daily GSR below demonstrate that the perfect fit was very close to the observed values. The showed values indicate that the FFNN-BP model shows good interpretation and good practicality for daily GSR.

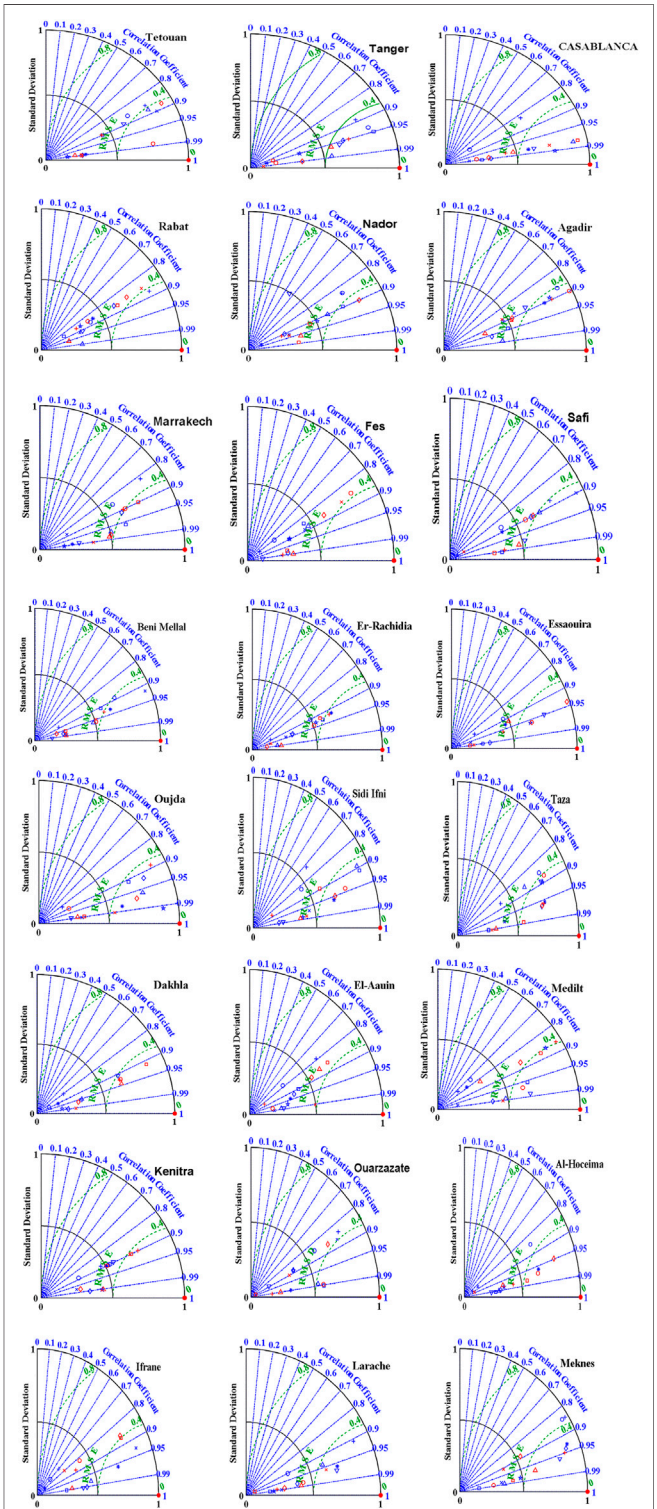

FIGURE 7 | Taylor diagrams of twenty-five study locations in Morocco.

TABLE 5 | Best five inputs parameters of 25 location in Morocco.

Location	Best input parameters	MBE	MBE(%)	RMSE	RMSE(%)	NRMSE	MAPE	TS	σ	σ(%)	R^2	A	b
Kenitra	03-Inputs	–5,6610	–0,2672	16,9567	0,3580	0,0710	0,0022	92,0634	39,8794	0,2540	0,9730	0,9161	0,1630
	05-Inputs	**–1,4153**	**–0,2663**	**11,3676**	**0,2400**	**0,0615**	**0,0019**	**89,8412**	**20,8181**	**0,2370**	**0,9910**	**0,9051**	**0,2100**
	08-Inputs	–28,3050	–0,2720	21,1722	0,4470	0,0716	0,0036	110,4124	30,1291	0,3430	0,9910	0,9011	0,1570
	14-Inputs	–25,0028	–0,2713	25,8139	0,5450	0,0946	0,0045	119,3137	37,7712	0,4300	0,9900	0,8241	0,0680
	15-Inputs	–26,4180	–0,2716	18,2355	0,3850	0,0713	0,0063	119,9677	24,7709	0,2820	0,9770	0,9211	0,1890
Casablanca	03-Inputs	–11,9980	–0,2662	26,3156	0,2700	0,0473	0,0041	40,1441	34,5014	0,2660	0,9870	0,9151	0,1630
	04-Inputs	–11,8750	–0,2665	15,2531	0,3220	0,0461	0,0032	82,4748	45,9631	0,2680	0,9830	0,9111	0,1480
	05-Inputs	**–10,0750**	**–0,2661**	**14,8482**	**0,2209**	**0,0355**	**0,0020**	**35,5846**	**25,7142**	**0,2550**	**0,9900**	**0,9191**	**0,1770**
	11-Inputs	–16,4500	–0,2674	20,0354	0,4230	0,0700	0,0033	114,9518	40,6531	0,3180	0,9815	0,8941	0,1640
	14-Inputs	–12,3000	–0,2664	19,2302	0,4060	0,0719	0,0063	102,9155	32,5677	0,3020	0,9850	0,9111	0,1570
Rabat	03-Inputs	–18,4500	–0,2786	24,9132	0,3100	0,0963	0,0023	84,7487	22,2150	0,3060	0,9540	0,9101	0,1690
	06-Inputs	**–13,9750**	**–0,2693**	**18,9460**	**0,2900**	0,0848	**0,0019**	27,2725	17,0628	**0,2950**	**0,9901**	**0,8891**	**0,1890**
	07-Inputs	–14,5250	–0,2787	19,1355	0,4040	0,0851	0,0029	92,0932	32,3520	0,3000	0,9130	0,9111	0,1380
	10-Inputs	–16,5750	–0,2781	20,1301	0,4250	0,0854	0,0039	108,6316	34,7245	0,3220	0,9090	0,9241	0,1480
	15-Inputs	–15,0500	–0,2794	18,7565	0,3960	0,0860	0,0052	102,8658	31,3814	0,2910	0,8550	0,8951	0,1310
Safi	04-Inputs	–24,3000	–0,3316	36,2822	0,6896	0,8980	0,0060	95,8265	35,5540	0,3030	0,9910	0,9041	0,2100
	07-Inputs	–36,0750	–0,3413	30,7050	0,6220	0,8680	0,0054	71,8319	45,8485	0,5190	0,9730	0,9211	0,1580
	10-Inputs	–36,4500	–0,3118	23,5471	0,4770	0,8291	0,0042	64,6377	43,7678	0,3730	0,9870	0,9161	0,1930
	12-Inputs	**–26,0750**	**–0,3051**	**22,5286**	**0,4580**	**0,7782**	**0,0032**	**47,7793**	**41,5384**	**0,3540**	**0,9910**	**0,9121**	**0,1970**
	15-Inputs	–30,3750	–0,3373	28,5823	0,5790	0,9279	0,0053	83,2165	55,7365	0,4750	0,9810	0,9051	0,2010
Agadir	04-Inputs	–18,4500	–0,2790	25,2765	0,4370	0,8478	0,0057	69,7631	33,5974	0,3130	0,9230	0,9091	0,1470
	05-Inputs	–29,0500	–0,4473	39,7985	0,4550	0,8827	0,0059	109,8439	34,1663	0,3510	0,9600	0,8831	0,1610
	06-Inputs	**–12,1800**	**–0,1795**	**16,6866**	**0,4210**	**0,8167**	**0,0055**	**46,0550**	**32,2508**	**0,2970**	**0,9870**	**0,8981**	**0,1330**
	13-Inputs	–17,1344	–0,2581	23,4741	0,4270	0,8284	0,0056	64,7886	50,8115	0,5220	0,9090	0,8901	0,1550
	15-Inputs	–16,1000	–0,2417	22,0570	0,4820	0,9351	0,0063	60,8773	46,3338	0,4760	0,9440	0,8681	0,1180
Essaouira	03-Inputs	–20,8250	–0,3027	30,1963	0,2550	0,4947	0,0033	86,0593	17,6010	0,1500	0,9900	0,9021	0,2390
	04-Inputs	–20,3000	–0,2947	29,4350	0,2630	0,5102	0,0034	83,8898	18,6571	0,1590	0,9640	0,9141	0,2500
	05-Inputs	**–14,5250**	**–0,2071**	**21,0613**	**0,2140**	**0,4152**	**0,0028**	**60,0246**	**14,6754**	**0,1300**	**0,9910**	**0,9101**	**0,2270**
	12-Inputs	–20,3000	–0,2947	29,4350	0,3570	0,6926	0,0046	83,8898	29,6870	0,2530	0,9910	0,9171	0,2530
	13-Inputs	–29,9750	–0,4416	43,4638	0,2860	0,5548	0,0037	97,7934	21,4732	0,1830	0,9890	0,9231	0,2540
Settat	05-Inputs	–23,8000	–0,3274	32,1300	0,3470	0,6732	0,0045	72,2925	16,8994	0,2530	0,9900	0,9101	0,3490
	09-Inputs	–19,8750	–0,2713	26,8313	0,3890	0,7547	0,0051	60,3703	18,0079	0,2385	0,9850	0,9041	0,3570
	12-Inputs	**–14,8765**	**–0,1999**	**20,0833**	**0,3330**	**0,6460**	**0,0043**	**45,1874**	**16,7949**	**0,2290**	**0,9920**	**0,9141**	**0,3570**
	14-Inputs	–26,3250	–0,3634	35,5388	0,3848	0,7465	0,0050	79,9622	16,8970	0,2440	0,9840	0,9171	0,2520
	15-Inputs	–20,1640	–0,2754	27,2214	0,4264	0,8272	0,0055	61,2482	18,8917	0,2610	0,9770	0,9241	0,2480
Dakhla	03-Inputs	–26,8200	–0,3937	30,8430	0,2880	0,5587	0,0037	69,3968	22,6946	0,1840	0,9830	0,9131	0,2330
	05-Inputs	–36,7280	–0,5440	42,2372	0,3460	0,6712	0,0045	95,0337	28,3963	0,2420	0,9850	0,9181	0,2510
	08-Inputs	–48,0040	–0,7151	55,2046	0,3650	0,7081	0,0047	113,1694	30,5084	0,2600	0,9860	0,8951	0,2240
	12-Inputs	**–23,6400**	**–0,3454**	**27,1860**	**0,2720**	**0,5277**	**0,0035**	**61,1685**	**21,9426**	**0,1800**	**0,9900**	**0,9021**	**0,2250**
	14-Inputs	–34,3640	–0,5082	39,5186	0,2990	0,5801	0,0039	88,9169	23,2005	0,1980	0,9740	0,9221	0,2380
Al-Auin	03-Inputs	–28,0920	–0,4130	32,3058	0,3310	0,6421	0,0043	72,6881	26,6362	0,2270	0,9690	0,9071	0,2470
	06-Inputs	–25,7456	–0,3774	29,6074	0,3320	0,6441	0,0043	66,6167	26,8709	0,2290	0,9900	0,9061	0,2320
	07-Inputs	–24,0548	–0,3517	27,6630	0,4150	0,8051	0,0054	62,2418	36,4927	0,3110	0,9640	0,9091	0,2420
	11-Inputs	–20,6184	–0,2996	23,7112	0,3200	0,6208	0,0042	53,3501	25,3454	0,2160	0,9860	0,9091	0,3500
	12-Inputs	**–17,1820**	**–0,2474**	**19,7593**	**0,2880**	**0,5587**	**0,0037**	**44,4584**	**24,8046**	**0,1840**	**0,9910**	**0,9031**	**0,2480**
Sidi Ifni	**05-Inputs**	**–10,0548**	**–0,1393**	**13,5740**	**0,3090**	**0,5995**	**0,0040**	**30,5415**	**24,0547**	**0,2050**	**0,9870**	**0,9081**	**0,2380**
	07-Inputs	–18,8728	–0,2731	25,4783	0,3410	0,6615	0,0044	57,3261	27,9269	0,2380	0,9860	0,9141	0,2490
	08-Inputs	–27,1092	–0,3981	36,5974	0,5010	0,9719	0,0065	82,3442	46,5840	0,3970	0,9840	0,9081	0,2940
	12-Inputs	–28,9638	–0,4262	39,1011	0,5120	0,9933	0,0067	87,9775	50,2215	0,4280	0,9830	0,9041	0,3480
	15-Inputs	–29,8092	–0,4390	40,2424	0,4810	0,9331	0,0063	90,5454	44,3545	0,3780	0,9860	0,9171	0,2500
Tanger	03-Inputs	–39,8670	–0,5917	39,0697	0,4640	0,9002	0,0060	87,9067	41,0690	0,3500	0,9910	0,9011	0,1510
	06-Inputs	–33,9150	–0,5013	33,2367	0,4590	0,8905	0,0060	74,7826	42,7690	0,5530	0,9870	0,8601	0,0990
	11-Inputs	–29,8765	–0,4401	29,2790	0,2360	0,4578	0,0031	65,8777	15,4889	0,1320	0,9860	0,9111	0,1550
	12-Inputs	**–29,7750**	**–0,4385**	**29,1795**	**0,1990**	**0,3861**	**0,0026**	**65,6539**	**10,3259**	**0,0880**	**0,9910**	**0,9211**	**0,1900**
	14-Inputs	–39,7280	–0,5895	38,9334	0,2780	0,5393	0,0036	87,6002	20,4172	0,1740	0,9760	0,9171	0,1660
Tetouan	03-Inputs	–35,9904	–0,5328	35,2706	0,3630	0,7042	0,0047	79,3588	30,5084	0,2600	0,9901	0,8961	0,2390
	08-Inputs	–39,7280	–0,5895	38,9334	0,2570	0,4986	0,0033	87,6002	17,9530	0,1530	0,9870	0,9021	0,2260
	12-Inputs	**–27,2592**	**–0,4003**	**26,7140**	**0,3610**	**0,7003**	**0,0047**	**60,1065**	**14,7364**	**0,1357**	**0,9910**	**0,9151**	**0,1510**
	13-Inputs	–30,8865	–0,4554	30,2688	0,3560	0,6906	0,0046	68,1047	29,5697	0,2520	0,9902	0,9211	0,1490
	15-Inputs	–33,9515	–0,5019	33,2725	0,3910	0,7585	0,0051	74,8631	24,1720	0,2060	0,9850	0,9001	0,1370
Al-Hoceima	**04-Inputs**	**–11,2680**	**–0,1577**	**22,3106**	**0,3740**	**0,7256**	**0,0049**	**50,1989**	**20,8818**	**0,2700**	**0,9920**	**0,9021**	**0,1490**
	05-Inputs	–11,9517	–0,1681	23,6644	0,4180	0,8109	0,0054	53,2448	36,8448	0,3140	0,9890	0,9181	0,1620
	06-Inputs	–14,9195	–0,2131	29,5406	0,4080	0,7915	0,0053	66,4664	27,4576	0,2340	0,9900	0,9151	0,1650
	07-Inputs	–15,3293	–0,2193	30,3520	0,4040	0,7838	0,0053	68,2920	35,2020	0,3000	0,9900	0,9091	0,1440

(Continued on following page)

TABLE 5 | (*Continued*) Best five inputs parameters of 25 location in Morocco.

Location	Best input parameters	MBE	MBE(%)	RMSE	RMSE(%)	NRMSE	MAPE	TS	σ	σ(%)	R^2	A	b
	15-Inputs	−19,9195	−0,2890	39,4406	0,4420	0,8575	0,0057	88,7414	39,7783	0,3390	0,9730	0,9131	0,1690
Larache	03-Inputs	−19,9195	−0,2890	17,5292	0,3370	0,6538	0,0044	56,9698	27,3402	0,2330	0,9850	0,9131	0,2450
	04-Inputs	**−7,9678**	**−0,1076**	**10,3390**	**0,2830**	**0,5490**	**0,0037**	**33,6018**	**21,0039**	**0,1790**	**0,9920**	**0,9191**	**0,2550**
	08-Inputs	−19,9195	−0,2890	17,5292	0,3120	0,6053	0,0041	56,9698	24,4067	0,2080	0,9910	0,9061	0,2460
	10-Inputs	−11,9517	−0,1681	10,5175	0,3920	0,7605	0,0051	34,1819	33,9113	0,2890	0,9860	0,9161	0,2690
	14-Inputs	−32,8229	−0,4848	28,8842	0,3710	0,7197	0,0048	93,8735	31,2124	0,2660	0,9900	0,9031	0,2210
Nador	03-Inputs	−31,9680	−0,4718	24,9350	0,3720	0,7217	0,0048	56,1038	31,4471	0,2680	0,9010	0,9081	0,1570
	05-Inputs	−26,6400	−0,3909	20,7792	0,4750	0,9215	0,0062	46,7532	43,0638	0,3670	0,9590	0,8581	0,1770
	11-Inputs	−23,1768	−0,3384	18,0779	0,3980	0,7721	0,0052	40,6753	34,4980	0,2940	0,9230	0,9211	0,1850
	12-Inputs	**−22,3776**	**−0,3263**	**17,4545**	**0,3460**	**0,6712**	**0,0045**	**39,2727**	**31,2383**	**0,2420**	**0,9860**	**0,9141**	**0,1400**
	15-Inputs	−39,9600	−0,5931	31,1688	0,3970	0,7702	0,0052	70,1298	34,3806	0,2930	0,9350	0,9261	0,0830
Oujda	03-Inputs	−53,2800	−0,7952	29,8368	0,3370	0,6538	0,0044	67,1328	27,3402	0,2330	0,9870	0,9211	0,2340
	07-Inputs	−47,9520	−0,7143	26,8531	0,4290	0,8323	0,0056	60,4195	38,2528	0,3260	0,9890	0,9121	0,2340
	12-Inputs	**−23,9760**	−0,3505	13,4266	**0,3130**	0,6072	0,0041	30,2098	26,9881	**0,2090**	**0,9910**	**0,9171**	**0,2500**
	13-Inputs	−29,3040	−0,4314	16,4102	0,3830	0,7430	0,0050	36,9230	32,7379	0,2790	0,9870	0,9101	0,2440
	15-Inputs	−39,9600	−0,5931	22,3776	0,4490	0,8711	0,0058	50,3496	42,3683	0,5450	0,9900	0,9101	0,2330
Taza	03-Inputs	−38,6280	−0,5729	21,6317	0,4550	0,8827	0,0059	48,6713	48,1243	0,5510	0,9870	0,9021	0,2210
	04-Inputs	−42,5707	−0,6327	23,8396	0,3600	0,6984	0,0047	53,6391	30,0390	0,2560	0,9900	0,9091	0,3600
	12-Inputs	**−25,8408**	**−0,3788**	**14,4708**	**0,2900**	**0,5626**	**0,0038**	**32,5594**	**28,4112**	**0,2160**	**0,9910**	**0,9101**	**0,2270**
	13-Inputs	−34,6320	−0,5122	19,3939	0,5020	0,9739	0,0065	43,6363	46,7013	0,3980	0,9740	0,8891	0,2290
	15-Inputs	−47,9520	−0,7143	26,8531	0,4240	0,8226	0,0055	60,4195	37,4315	0,3190	0,9900	0,9041	0,2040
Meknes	03-Inputs	−24,7752	−0,3626	11,7930	0,5320	1,0321	0,0069	63,0925	49,7522	0,4240	0,9830	0,8701	0,1830
	04-Inputs	−20,7792	−0,3020	9,8909	0,4560	0,8846	0,0059	52,9163	29,9957	0,1520	0,9880	0,9211	0,2530
	06-Inputs	−17,0496	−0,2454	8,1156	0,4720	0,9157	0,0061	43,4185	31,4471	0,2680	0,9860	0,9101	0,2540
	07-Inputs	**−15,9840**	**−0,2293**	**7,6084**	**0,4190**	**0,8129**	**0,0054**	**40,7049**	**31,0057**	**0,2550**	**0,9880**	**0,9191**	**0,2510**
	11-Inputs	−31,9680	−0,4718	15,2168	0,4370	0,8478	0,0057	81,4097	39,0742	0,3330	0,9820	0,9051	0,3600
Beni-Mellal	05-Inputs	−26,3949	−0,3872	12,5640	0,3570	0,6926	0,0046	67,2173	29,6870	0,2530	0,9820	0,9211	0,1690
	07-Inputs	**−20,7792**	**−0,3020**	**9,8909**	**0,2450**	**0,4753**	**0,0032**	**52,9163**	**16,5449**	**0,1410**	**0,9900**	**0,9111**	**0,3810**
	08-Inputs	−26,1072	−0,3829	12,4270	0,3380	0,6557	0,0044	66,4846	27,3402	0,2330	0,9750	0,8971	0,2310
	14-Inputs	−35,6976	−0,5284	16,9921	0,3580	0,6945	0,0047	90,9075	29,8044	0,2540	0,9880	0,9151	0,2490
	15-Inputs	−49,8168	−0,7426	23,7128	0,2850	0,5529	0,0037	118,8011	21,2385	0,1810	0,9580	0,9101	0,2180
Ifrane	04-Inputs	−23,9760	−0,3505	11,4126	0,4870	0,9448	0,0063	61,0573	44,9412	0,3830	0,9910	0,9071	0,2240
	05-Inputs	−15,9840	−0,2293	7,6084	0,3940	0,7644	0,0051	40,7049	34,0286	0,2900	0,9870	0,9141	0,2470
	06-Inputs	−18,6480	−0,2697	8,8764	0,4570	0,8866	0,0059	47,4890	53,2724	0,4540	0,9770	0,9121	0,3530
	07-Inputs	**−13,3200**	**−0,1888**	**6,3403**	**0,4190**	**0,8129**	**0,0054**	**33,9207**	**30,0211**	**0,2150**	**0,9910**	**0,9131**	**0,2390**
	15-Inputs	−23,9760	−0,3505	11,4126	0,4890	0,9487	0,0064	61,0573	28,7483	0,2450	0,9900	0,9181	0,2440
Fes	05-Inputs	−13,3200	−0,1888	6,3403	0,3840	07,450	0,0050	33,9207	32,9725	0,2810	0,9840	0,9091	0,2430
	07-Inputs	**−9,8568**	**−0,1363**	**4,6918**	**0,2070**	**0,4016**	**0,0027**	**25,1013**	**12,0860**	**0,1030**	**0,9910**	**0,9101**	**0,1920**
	10-Inputs	−21,3120	−0,3101	10,1445	0,3810	0,7391	0,0050	54,2731	32,5032	0,2770	0,9730	0,9081	0,1420
	13-Inputs	−18,3816	−0,2656	8,7496	0,4200	0,8148	0,0055	46,8106	36,8448	0,3140	0,9900	0851	0,1490
	15-Inputs	−15,9840	−0,2293	7,6084	0,3460	0,6712	0,0045	40,7049	28,3963	0,2420	0,9880	0,9131	0,1620
Medilt	03-Inputs	−55,9440	−0,8356	26,6293	0,5010	0,9719	0,0065	115,8376	23,5280	0,4970	0,9900	0,9031	0,2320
	05-Inputs	−53,2800	−0,7952	25,3613	0,4940	0,9584	0,0064	110,3216	45,8799	0,3910	0,9890	0,9161	0,2370
	06-Inputs	−47,9520	−0,7143	22,8252	0,4900	0,9506	0,0064	99,2894	56,7926	0,4840	0,9870	0,8931	0,2130
	07-Inputs	−45,2880	−0,6739	21,5571	0,5060	0,9816	0,0066	93,7733	16,7796	0,1430	0,9770	0,9241	0,2540
	12-Inputs	**−39,9600**	**−0,5931**	**19,0210**	**0,4607**	**0,8938**	**0,0060**	**82,7412**	**12,6311**	**0,1020**	**0,9910**	**0,8811**	**0,3170**
Marrakech	07-Inputs	−63,9360	−0,9569	30,4335	0,4790	0,9293	0,0062	132,3859	43,7678	0,3730	0,9910	0,8791	0,1270
	08-Inputs	−51,9480	−0,7750	24,7272	0,3300	0,6402	0,0043	107,5635	26,5188	0,2260	0,9860	0,9111	0,1500
	09-Inputs	−47,9520	−0,7143	22,8252	0,3780	0,7333	0,0049	99,2894	32,1512	0,2740	0,9850	0,9161	0,1750
	12-Inputs	**−36,2304**	**−0,5365**	**17,2457**	**0,2740**	**0,5316**	**0,0036**	**75,0187**	**19,9478**	**0,1700**	**0,9920**	**0,9121**	**0,1690**
	15-Inputs	−53,2800	−0,7952	25,3613	0,4910	0,9525	0,0064	110,3216	57,2619	0,4880	0,9830	0,9191	0,1620
Ouarzazate	**04-Inputs**	**−13,8528**	**−0,1969**	**6,5939**	**0,2780**	**0,5393**	**0,0036**	**35,2775**	**39,8012**	**0,2174**	**0,9910**	**0,8801**	**0,1830**
	06-Inputs	−15,9840	−0,2293	7,6084	0,3360	0,6518	0,0044	40,7049	45,7829	0,2320	0,9900	0,9131	0,1600
	09-Inputs	−21,3120	−0,3101	10,1445	0,6320	1,2261	0,0082	54,2731	62,0729	0,5290	0,9860	0,9121	0,1350
	11-Inputs	−23,7096	−0,3465	11,2858	0,6740	1,3076	0,0088	60,3789	55,5811	0,5710	0,9890	0,9161	0,1600
	15-Inputs	−30,9024	−0,4556	14,7095	0,4190	0,8129	0,0054	78,6961	36,8448	0,3140	0,9890	0,9001	0,1310
Er-Rachidia	03-Inputs	−14,6520	−0,2090	6,9744	0,3770	0,7314	0,0049	37,3128	32,0338	0,2730	0,9440	0,9121	0,2540
	04-Inputs	**−12,6806**	**−0,1791**	**6,0360**	**0,2980**	**0,5781**	**0,0039**	**32,2925**	**16,5560**	**0,1078**	**0,9880**	**0,9201**	**0,2560**
	06-Inputs	−15,9840	−0,2293	7,6084	0,3520	0,6829	0,0046	40,7049	17,3663	0,1480	0,9550	0,9071	0,3680
	12-Inputs	−20,7792	−0,3020	9,8909	0,3290	0,6383	0,0043	52,9163	26,4015	0,2250	0,9910	0,9111	0,2490
	14-Inputs	−22,1112	−0,3222	10,5249	0,4180	0,8109	0,0054	56,3084	20,2168	0,1140	0,9830	0,9161	0,2500

The values displayed in bold show the lowest values of the statistical performance indicators and the highest value of the correlation coefficient R^2 *among the five best input parameters for each city studied.*

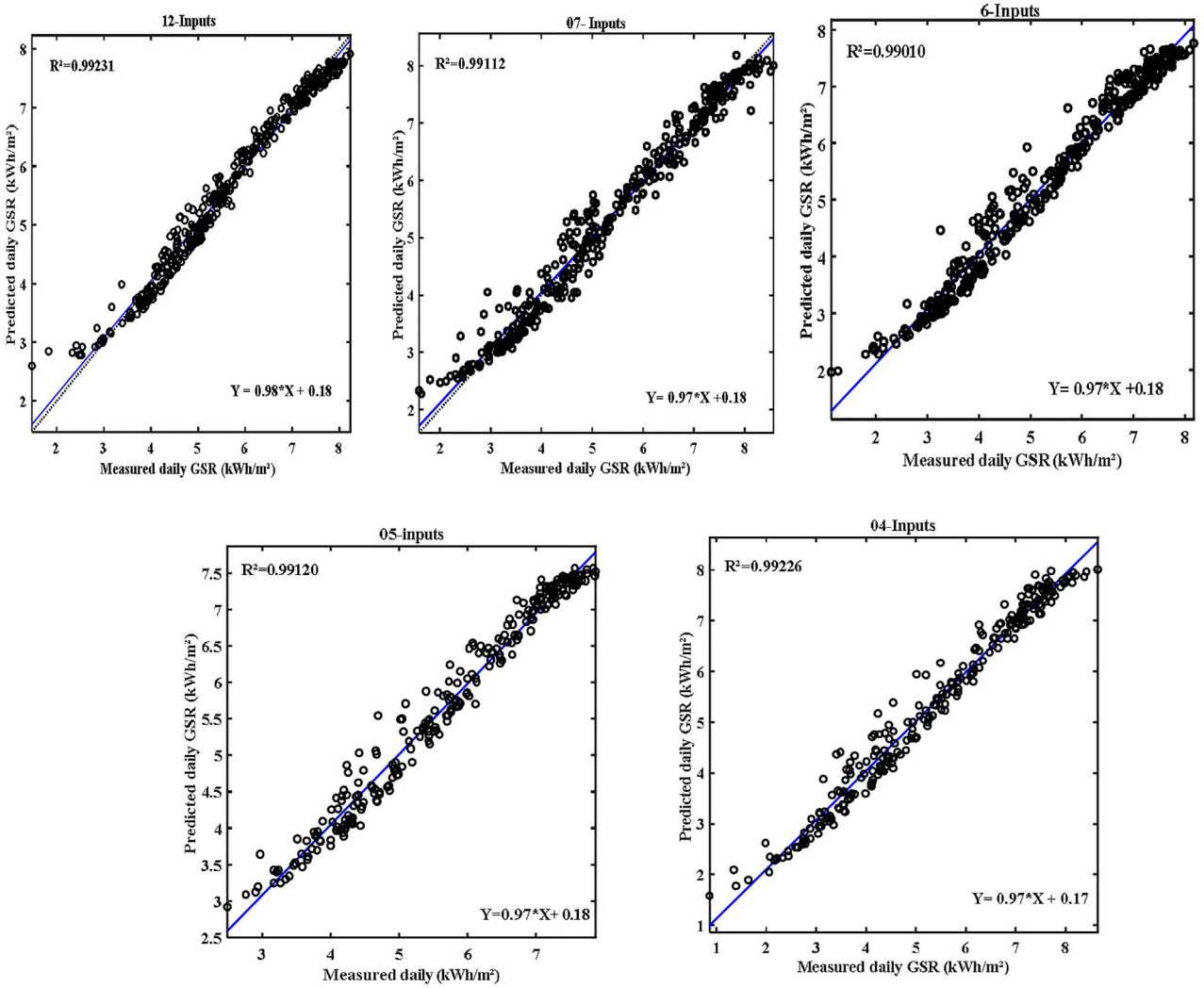

FIGURE 8 | Scatter plot of daily GSR predicted values by the best six inputs vs. measured values.

Table 6 presents a brief comparison of multiple studies for different locations using several meteorological, astronomical, and geographical data as input parameters between the present study and others previously cited in the literature in order to predict the daily global solar radiation. The comparison metric is based on the coefficient of determination (R^2). Therefore, most of the cited studies for the prediction of daily global solar radiation used different algorithms have generally presented close results to another one. According to the statistical metrics, it can be noted that the highest value of the coefficient of determination corresponds to the appropriate models. As we can see from **Table 6**, it clearly appears that the current study presents the appropriate model compared to other studies cited in the literature. The R^2 value of the proposed model is 99.20, which ensures that the proposed model performs better than other existing methods.

Figure 9 ranks the twenty-five studied locations in terms of predicted outputs. The best results of the selected input parameters for Ouarzazate, Al-Hoceima, and Lareche cities are K_t, TOA, T_{max}, and T_{ratio}. The best results of the selected input parameters for Kenitra, Casablanca, Essaouira, and Sidi Ifni are K_t, TOA, T_{max} T_{ratio}, and ΔT. The K_t, TOA, T_{max} T_{ratio}, ΔT, and $T_{average}$ are the selected input parameters for Rabat and Agadir city. The best seven input parameters for the considered location (Meknes, Beni-Mellal, Ifrane, and Fes) are K_t, TOA, T_{max} T_{ratio}, ΔT, $T_{average}$, and T_{min}. Er-Rachidia, Marrakech, Midelt, Taza, Oujda, Nador, Tetouan, Tanger, Al-Auin, Dakhla, and Settat City are the locations considered for twelve input parameters (K_t, TOA, T_{max} T_{ratio}, ΔT, $T_{average}$, Alt, Long, Lat, δ, D_{length}, D_{number}, W_s, and R_h). The analysis indicator shows that the increase in input numbers improves the accuracy and adaptability of the ANN model.

In order to compare the agreement between measured daily average global solar radiation and the predicted one for twenty-five Moroccan selected locations, the relative difference values are 4.84 and 6.75% for the ANN model and the mean, max, min value

TABLE.6 | Metrics comparison of current study with the existing literature studies in the prediction of daily global solar radiation.

References	Studied locations	Input parameters to ANNs model	R^2 (%)
Yıldız et al. (2013)	Turkey	Latitude, longitude, altitude, month, and meteorological land surface temperature	82.37
Rahimikhoob, (2010)	Iran	Maximum and minimum air temperature and extraterrestrial radiation	88.9
Fadare, (2009)	Nigeria	Latitude, longitude, altitude, month, mean sunshine duration, mean temperature, and relative humidity	90
Benghanem et al. (2009)	Saudi Arabia	humidity, sunshine duration and the day of the year	97.65
Jiang, (2009)	China	Latitude, altitude, and mean sunshine	97
Marzouq et al. (2018)	Morocco	Top of the atmosphere, maximum temperature, solar altitude angle, and minimum relative humidity	95.99
Bounoua et al. (2021)	Morocco	Day of the year, daily mean air temperature, relative humidity, wind speed, wind direction, air vapor pressure, extraterrestrial radiation, maximum and minimum air temperature, gradient temperature, root square temperature gradient, and temperature ratio	95.04
Wang et al. (2016)	China	Air temperature, air pressure, maximum air temperature, extraterrestrial radiation, latitude, longitude, altitude, relative humidity, and water vapor pressure	90
El Mghouchi et al. (2019)	Morocco	Geographical coordinates, sun declination, day length, day number, clearness index, top of atmosphere, average ambient temperature, maximum and minimum temperature, difference temperature, temperature ratio, relative humidity, and wind speed	99
B. Belmahdi et al.	Morocco	Clearness index, day number, day length, minimal temperature, maximal temperature, average temperature, difference temperature, ratio temperature, average humidity, top outside atmosphere radiation, average wind speed, altitude, longitude, latitude, and solar declination	99.20

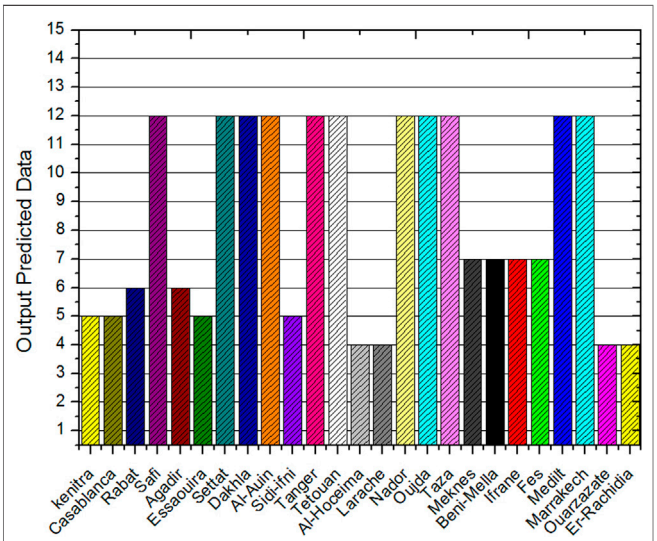

FIGURE 9 | Output predicted data and the best selected parameters for all Moroccan cities.

of the predicted and measured model are 5.493, 5.09, 5.19 and 5.796, 5.39, and 5.49, respectively, as presented in **Figure 9**, revealing the high accuracy of the ANN model in simulation. The selected model also seems well adapted to predict daily global solar radiation in other study locations successfully.

CONCLUSION

The article presents the FFNN-BP model and its application in predicting the daily global solar radiation. A feedforward backpropagation is employed using different metrological and geographical coordinates. The proposed neural network runs with ten neurons and the log-sigmoid transfer function of the hidden layer and the output layers are employed for the prediction model. Geographical and meteorological parameters, such as K_t, TOA, T_{max} T_{ratio}, ΔT, $T_{average}$, T_{min}, Alt, Long, Lat, δ, D_{length}, D_{number}, W_s, and R_h , have been used as input variables and daily global solar radiation as outputs variables. Each step was increasing the number of inputs to determine the most accurate and suitable parameters. As the results have shown, all parameters are qualified to demonstrate their adaptability and efficiency for the study weather conditions. The best twelve, seven, six, five, and four input parameters with the proposed model in this study can also be preferred to predict daily GSR with high logical accuracy and faster performance analysis. This obtained result is an indication of a good matching between measured and predicted global solar radiation. Following the same procedures, this technique could be used to predict other outputs data of different locations where measurement instrumentation is unavailable or costly to obtain. The statistical error metrics calculated for each predicted value and the Taylor diagrams show the good ability of the proposed models in predicting daily solar radiation. This result can be useful for installing several solar energy capacities, such as photovoltaic farms or solar collectors.

DATA AVAILABILITY STATEMENT

The raw data supporting the conclusions of this article will be made available by the authors without undue reservation.

AUTHOR CONTRIBUTIONS

BB collected the data, conceived the analysis procedure, and provided the analysis tools, the methodology, and the software. BB and ML designed the analysis procedure and supervised it. BB and ML was responsible for the original

draft preparation. BB, ML, and AB contributed to the investigation. MA, DC, PC, and AB reviewed the manuscript. All authors read and approved the final manuscript.

REFERENCES

Aarich, N., Erraissi, N., Akhsassi, M., Bennouna, A., Asselman, A., Barhdadi, A., et al. (2018). Photovoltaic DC Yield Maps for All Morocco Validated with Ground Measurements. *Energy Sustain. Dev.* 47, 158–169. doi:10.1016/j.esd.2018.10.003

Al-Dahidi, S., Ayadi, O., Adeeb, J., and Louzazni, M. (2019). Assessment of Artificial Neural Networks Learning Algorithms and Training Datasets for Solar Photovoltaic Power Production Prediction. *Front. Energ. Res.* 7, 130. doi:10.3389/fenrg.2019.00130

Al-Alawi, S. M., and Al-Hinai, H. A. (1998). An ANN-Based Approach for Predicting Global Radiation in Locations with No Direct Measurement Instrumentation. *Renew. Energ.* 14 (1), 199–204. doi:10.1016/s0960-1481(98)00068-8

Alam, S., Kaushik, S. C., and Garg, S. N. (2006). Computation of Beam Solar Radiation at normal Incidence Using Artificial Neural Network. *Renew. Energ.* 31 (10), 1483–1491. doi:10.1016/j.renene.2005.07.010

Allouhi, A., Jamil, A., Kousksou, T., El Rhafiki, T., Mourad, Y., and Zeraouli, Y. (2015). Solar Domestic Heating Water Systems in Morocco: An Energy Analysis. *Energy Convers. Manag.* 92, 105–113. doi:10.1016/j.enconman.2014.12.055

Alsina, E. F., Bortolini, M., Gamberi, M., and Regattieri, A. (2016). Artificial Neural Network Optimisation for Monthly Average Daily Global Solar Radiation Prediction. *Energ. Convers. Manag.* 120, 320–329. doi:10.1016/j.enconman.2016.04.101

Amirian, E., Dejam, M., and Chen, Z. (2018). Performance Forecasting for Polymer Flooding in Heavy Oil Reservoirs. *Fuel* 216, 83–100. doi:10.1016/j.fuel.2017.11.110

Battiti, R. (1992). First- and Second-Order Methods for Learning: Between Steepest Descent and Newton's Method. *Neural Comput.* 4 (2), 141–166. doi:10.1162/neco.1992.4.2.141

Bebis, G., and Georgiopoulos, M. (1994). Feed-forward Neural Networks. *IEEE Potentials* 13 (4), 27–31. doi:10.1109/45.329294

Belmahdi, B., and Bouardi, A. E. (2020). Simulation and Optimization of Microgrid Distributed Generation: a Case Study of University Abdelmalek Essaâdi in Morocco. *Proced. Manuf.* 46, 746–753. doi:10.1016/j.promfg.2020.03.105

Belmahdi, B., and El Bouardi, A. (2020). Solar Potential Assessment Using PVsyst Software in the Northern Zone of Morocco. *Proced. Manuf.* 46, 738–745. doi:10.1016/j.promfg.2020.03.104

Belmahdi, B., Louzazni, M., and El Bouardi, A. (2020). One Month-Ahead Forecasting of Mean Daily Global Solar Radiation Using Time Series Models. *Optik (Stuttg).* 219, 165207. doi:10.1016/j.ijleo.2020.165207

Belmahdi, B., Louzazni, M., and El Bouardi, A. (2020). A Hybrid ARIMA–ANN Method to Forecast Daily Global Solar Radiation in Three Different Cities in Morocco. *Eur. Phys. J. Plus* 135 (11), 925. doi:10.1140/epjp/s13360-020-00920-9

Benghanem, M., Mellit, A., and Alamri, S. N. (2009). ANN-based Modelling and Estimation of Daily Global Solar Radiation Data: A Case Study. *Energ. Convers. Manag.* 50 (7), 1644–1655. doi:10.1016/j.enconman.2009.03.035

Boland, J., Scott, L., and Luther, M. (2001). Modelling the Diffuse Fraction of Global Solar Radiation on a Horizontal Surface. *Environmetrics* 12 (2), 103–116. doi:10.1002/1099-095x(200103)12:2<103:aid-env447>3.0.co;2-2

Bouhal, T., Agrouaz, Y., Kousksou, T., Allouhi, A., El Rhafiki, T., Jamil, A., et al. (2018). Technical Feasibility of a Sustainable Concentrated Solar Power in Morocco through an Energy Analysis. *Renew. Sustain. Energ. Rev.* 81 (1), 1087–1095. doi:10.1016/j.rser.2017.08.056

Bounoua, Z., Ouazzani Chahidi, L., and Mechaqrane, A. (2021). Estimation of Daily Global Solar Radiation Using Empirical and Machine-Learning Methods: A Case Study of Five Moroccan Locations. *Sustain. Mater. Technol.* 28, e00261. doi:10.1016/j.susmat.2021.e00261

Celik, A. N., and Muneer, T. (2013). Neural Network Based Method for Conversion of Solar Radiation Data. *Energ. Convers. Manag.* 67, 117–124. doi:10.1016/j.enconman.2012.11.010

Chakraborty, K., Mehrotra, K., Mohan, C. K., and Ranka, S. (1992). Forecasting the Behavior of Multivariate Time Series Using Neural Networks. *Neural Networks* 5 (6), 961–970. doi:10.1016/s0893-6080(05)80092-9

Chiteka, K., and Enweremadu, C. C. (2016). Prediction of Global Horizontal Solar Irradiance in Zimbabwe Using Artificial Neural Networks. *J. Clean. Prod.* 135, 701–711. doi:10.1016/j.jclepro.2016.06.128

Durna, B., and Şahin, A. D. (2020). Mapping of Daylight Illumination Levels Using Global Solar Radiation Data in and Around Istanbul, Turkey. *Weather* 75 (1), 19–25. doi:10.1002/wea.3386

El Mghouchi, Y., Ajzoul, T., and El Bouardi, A. (2016). Prediction of Daily Solar Radiation Intensity by Day of the Year in Twenty-Four Cities of Morocco. *Renew. Sustain. Energ. Rev.* 53, 823–831. doi:10.1016/j.rser.2015.09.059

El Mghouchi, Y., Chham, E., Zemmouri, E. M., and El Bouardi, A. (2019). Assessment of Different Combinations of Meteorological Parameters for Predicting Daily Global Solar Radiation Using Artificial Neural Networks. *Build. Environ.* 149, 607–622. doi:10.1016/j.buildenv.2018.12.055

Elminir, H. K., Azzam, Y. A., and Younes, F. I. (2007). Prediction of Hourly and Daily Diffuse Fraction Using Neural Network, as Compared to Linear Regression Models. *Energy* 32 (8), 1513–1523. doi:10.1016/j.energy.2006.10.010

Fadare, D. A. (2009). Modelling of Solar Energy Potential in Nigeria Using an Artificial Neural Network Model. *Appl. Energ.* 86 (9), 1410–1422. doi:10.1016/j.apenergy.2008.12.005

Feng, L., Lin, A., Wang, L., Qin, W., and Gong, W. (2018). Evaluation of sunshine-based Models for Predicting Diffuse Solar Radiation in China. *Renew. Sustain. Energ. Rev.* 94, 168–182. doi:10.1016/j.rser.2018.06.009

Gairaa, K., Khellaf, A., Messlem, Y., and Chellali, F. (2016). Estimation of the Daily Global Solar Radiation Based on Box-Jenkins and ANN Models: A Combined Approach. *Renew. Sustain. Energ. Rev.* 57, 238–249. doi:10.1016/j.rser.2015.12.111

George, D., and Huerta, E. A. (2018). Deep Neural Networks to Enable Real-Time Multimessenger Astrophysics. *Phys. Rev. D* 97 (4), 44039. doi:10.1103/physrevd.97.044039

Gueymard, C. A. (2014). A Review of Validation Methodologies and Statistical Performance Indicators for Modeled Solar Radiation Data: Towards a Better Bankability of Solar Projects. *Renew. Sustain. Energ. Rev.* 39, 1024–1034. doi:10.1016/j.rser.2014.07.117

Haykin, S. (1988). *Neural Networks: A Comprehensive Foundation*. 2nd Edition. Prentice-Hall.

Hontoria, L., Aguilera, J., and Zufiria, P. (2005). An Application of the Multilayer Perceptron: Solar Radiation Maps in Spain. *Sol. Energ.* 79 (5), 523–530. doi:10.1016/j.solener.2004.11.013

Huang, S.-J., and Shih, K.-R. (2003). Short-term Load Forecasting via ARMA Model Identification Including Non-Gaussian Process Considerations. *IEEE Trans. Power Syst.* 18 (2), 673–679. doi:10.1109/tpwrs.2003.811010

Jiang, Y. (2009). Computation of Monthly Mean Daily Global Solar Radiation in China Using Artificial Neural Networks and Comparison with Other Empirical Models. *Energy* 34 (9), 1276–1283. doi:10.1016/j.energy.2009.05.009

Kaba, K., Sarıgül, M., Avcı, M., and Kandırmaz, H. M. (2018). Estimation of Daily Global Solar Radiation Using Deep Learning Model. *Energy* 162, 126–135. doi:10.1016/j.energy.2018.07.202

Kamruzzaman, J., Begg, R., and Sarker, R. A. (2006). *Artificial Neural Networks in Finance and Manufacturing*. Idea Group Pub.

Kaplan, Y. A. (2018). A New Model for Predicting the Global Solar Radiation. *Environ. Prog. Sustain. Energ.* 37 (2), 870–880. doi:10.1002/ep.12721

Kashyap, Y., Bansal, A., and Sao, A. K. (2015). Solar Radiation Forecasting with Multiple Parameters Neural Networks. *Renew. Sustain. Energ. Rev.* 49, 825–835. doi:10.1016/j.rser.2015.04.077

Khan, S. A. R., Zaman, K., and Zhang, Y. (2016). The Relationship between Energy-Resource Depletion, Climate Change, Health Resources and the Environmental Kuznets Curve: Evidence from the Panel of Selected Developed Countries. *Renew. Sustain. Energ. Rev.* 62, 468–477. doi:10.1016/j.rser.2016.04.061

Khare, M., and Nagendra, S. M. S. (2007). *Artificial Neural Networks in Vehicular Pollution Modelling*. Springer.

Khatib, T., Mohamed, A., Sopian, K., and Mahmoud, M. (2012). Solar Energy Prediction for Malaysia Using Artificial Neural Networks. *Int. J. Photoenergy* 2012, 419504. doi:10.1155/2012/419504

Khwaja, A. S., Anpalagan, A., Naeem, M., and Venkatesh, B. (2020). Joint Bagged-Boosted Artificial Neural Networks: Using Ensemble Machine Learning to Improve Short-Term Electricity Load Forecasting. *Electr. Power Syst. Res.* 179, 106080. doi:10.1016/j.epsr.2019.106080

Lam, J. C., Wan, K. K. W., and Yang, L. (2008). Solar Radiation Modelling Using ANNs for Different Climates in China. *Energ. Convers. Manag.* 49 (5), 1080–1090. doi:10.1016/j.enconman.2007.09.021

Li, H., Cao, F., Bu, X., and Zhao, L. (2015). Models for Calculating Daily Global Solar Radiation from Air Temperature in Humid Regions-A Case Study. *Environ. Prog. Sustain. Energ.* 34 (2), 595–599. doi:10.1002/ep.12018

Liu, Y., Yang, L., Zheng, W., Liu, T., Zhang, X., and Liu, J. (2018). A Novel Building Energy Efficiency Evaluation index: Establishment of Calculation Model and Application. *Energ. Convers. Manag.* 166, 522–533. doi:10.1016/j.enconman.2018.03.090

Louzazni, M., Mosalam, H., and Khouya, A. (2020). A Non-linear Auto-Regressive Exogenous Method to Forecast the Photovoltaic Power Output. *Sustain. Energ. Technol. Assessments* 38, 100670. doi:10.1016/j.seta.2020.100670

Marzouq, M., Bounoua, Z., Mechaqrane, A., Fadili, H. E., Lakhliai, Z., and Zenkouar, K. (2018). ANN-based Modelling and Prediction of Daily Global Solar Irradiation Using Commonly Measured Meteorological Parameters. *IOP Conf. Ser. Earth Environ. Sci.* 161 (1), 012017. doi:10.1088/1755-1315/161/1/012017

Mba, L., Meukam, P., and Kemajou, A. (2016). Application of Artificial Neural Network for Predicting Hourly Indoor Air Temperature and Relative Humidity in Modern Building in Humid Region. *Energy Build.* 121, 32–42. doi:10.1016/j.enbuild.2016.03.046

Mehleri, E. D., Zervas, P. L., Sarimveis, H., Palyvos, J. A., and Markatos, N. C. (2010). A New Neural Network Model for Evaluating the Performance of Various Hourly Slope Irradiation Models: Implementation for the Region of Athens. *Renew. Energ.* 35 (7), 1357–1362. doi:10.1016/j.renene.2009.11.005

Mehleri, E. D., Zervas, P. L., Sarimveis, H., Palyvos, J. A., and Markatos, N. C. (2010). Determination of the Optimal Tilt Angle and Orientation for Solar Photovoltaic Arrays. *Renew. Energ.* 35 (11), 2468–2475. doi:10.1016/j.renene.2010.03.006

Mellit, A., Benghanem, M., Arab, A. H., and Guessoum, A. (2005). A Simplified Model for Generating Sequences of Global Solar Radiation Data for Isolated Sites: Using Artificial Neural Network and a Library of Markov Transition Matrices Approach. *Sol. Energ.* 79 (5), 469–482. doi:10.1016/j.solener.2004.12.006

Kumar, M., and Kumar, A. (2017). Performance Assessment and Degradation Analysis of Solar Photovoltaic Technologies: A Review. *Renew. Sustain. Energ. Rev.* 78, 554–587. doi:10.1016/j.rser.2017.04.083

Moreno, A., Gilabert, M. A., and Martínez, B. (2011). Mapping Daily Global Solar Irradiation over Spain: A Comparative Study of Selected Approaches. *Sol. Energ.* 85 (9), 2072–2084. doi:10.1016/j.solener.2011.05.017

Muneer, T., Younes, S., and Munawwar, S. (2007). Discourses on Solar Radiation Modeling. *Renew. Sustain. Energ. Rev.* 11 (4), 551–602. doi:10.1016/j.rser.2005.05.006

Notton, G., Paoli, C., Vasileva, S., Nivet, M. L., Canaletti, J.-L., and Cristofari, C. (2012). Estimation of Hourly Global Solar Irradiation on Tilted Planes from Horizontal One Using Artificial Neural Networks. *Energy* 39 (1), 166–179. doi:10.1016/j.energy.2012.01.038

Owusu, P. A., and Asumadu-Sarkodie, S. (2016). A Review of Renewable Energy Sources, Sustainability Issues and Climate Change Mitigation. *Cogent Eng.* 3 (1), 1167990. doi:10.1080/23311916.2016.1167990

Pacheco-Vega, A., Sen, M., Yang, K. T., and McClain, R. L. (2001). Neural Network Analysis of Fin-Tube Refrigerating Heat Exchanger with Limited Experimental Data. *Int. J. Heat Mass. Transf.* 44 (4), 763–770. doi:10.1016/s0017-9310(00)00139-3

Polo, J., Fernández-Peruchena, C., Salamalikis, V., Mazorra-Aguiar, L., Turpin, M., Martín-Pomares, L., et al. (2020). Benchmarking on Improvement and Site-Adaptation Techniques for Modeled Solar Radiation Datasets. *Sol. Energ.* 201, 469–479. doi:10.1016/j.solener.2020.03.040

Rahimikhoob, A. (2010). Estimating Global Solar Radiation Using Artificial Neural Network and Air Temperature Data in a Semi-arid Environment. *Renew. Energ.* 35 (9), 2131–2135. doi:10.1016/j.renene.2010.01.029

Rajendran, P., and Smith, H. (2016). Modelling of Solar Irradiance and Daylight Duration for Solar-Powered UAV Sizing. *Energy Explor. Exploit.* 34 (2), 235–243. doi:10.1177/0144598716629874

Siva Krishna Rao, D. V., Premalatha, M., and Naveen, C. (2018). Analysis of Different Combinations of Meteorological Parameters in Predicting the Horizontal Global Solar Radiation with ANN Approach: A Case Study. *Renew. Sustain. Energ. Rev.* 91, 248–258. doi:10.1016/j.rser.2018.03.096

Riahi-Madvar, H., Ayyoubzadeh, S. A., and Atani, M. G. (2011). Developing an Expert System for Predicting Alluvial Channel Geometry Using ANN. *Expert Syst. Appl.* 38 (1), 215–222. doi:10.1016/j.eswa.2010.06.047

Sayigh, A. (2017). *Photovoltaics for Sustainable Electricity and Buildings*. Springer International Publishing.

Sharifi, S. S., Rezaverdinejad, V., and Nourani, V. (2016). Estimation of Daily Global Solar Radiation Using Wavelet Regression, ANN, GEP and Empirical Models: A Comparative Study of Selected Temperature-Based Approaches. *J. Atmos. Solar Terrestrial Phys.* 149, 131–145. doi:10.1016/j.jastp.2016.10.008

Shekari Beidokhti, R., and Malek, A. (2009). Solving Initial-Boundary Value Problems for Systems of Partial Differential Equations Using Neural Networks and Optimization Techniques. *J. Franklin Inst.* 346 (9), 898–913. doi:10.1016/j.jfranklin.2009.05.003

Šimelytė, A. (2020). "Chapter 13 - Promotion of Renewable Energy in Morocco," in *Energy Transformation Towards Sustainability*. Editors M. Tvaronavičienė and S. Ślusarczyk (Elsevier), 249–287.

Sözen, A., Arcaklioğlu, E., Özalp, M., and Kanit, E. G. (2004). Use of Artificial Neural Networks for Mapping of Solar Potential in Turkey. *Appl. Energ.* 77 (3), 273–286. doi:10.1016/s0306-2619(03)00137-5

Sözen, A., Arcaklıoğlu, E., Özalp, M., and Çağlar, N. (2005). Forecasting Based on Neural Network Approach of Solar Potential in Turkey. *Renew. Energ.* 30 (7), 1075–1090. doi:10.1016/j.renene.2004.09.020

Sterjovski, Z., Nolan, D., Carpenter, K. R., Dunne, D. P., and Norrish, J. (2005). Artificial Neural Networks for Modelling the Mechanical Properties of Steels in Various Applications. *J. Mater. Process. Technol.* 170 (3), 536–544. doi:10.1016/j.jmatprotec.2005.05.040

Tagliaferri, F., Viola, I. M., and Flay, R. G. J. (2015). Wind Direction Forecasting with Artificial Neural Networks and Support Vector Machines. *Ocean Eng.* 97, 65–73. doi:10.1016/j.oceaneng.2014.12.026

Wang, L., Kisi, O., Zounemat-Kermani, M., Salazar, G. A., Zhu, Z., and Gong, W. (2016). Solar Radiation Prediction Using Different Techniques: Model Evaluation and Comparison. *Renew. Sustain. Energ. Rev.* 61, 384–397. doi:10.1016/j.rser.2016.04.024

Yadav, A. K., and Chandel, S. S. (2014). Solar Radiation Prediction Using Artificial Neural Network Techniques: A Review. *Renew. Sustain. Energ. Rev.* 33, 772–781. doi:10.1016/j.rser.2013.08.055

Yadav, A. K., Malik, H., and Chandel, S. S. (2014). Selection of Most Relevant Input Parameters Using WEKA for Artificial Neural Network Based Solar Radiation Prediction Models. *Renew. Sustain. Energ. Rev.* 31, 509–519. doi:10.1016/j.rser.2013.12.008

Yalcintas, M., and Akkurt, S. (2005). Artificial Neural Networks Applications in Building Energy Predictions and a Case Study for Tropical Climates. *Int. J. Energ. Res.* 29 (10), 891–901. doi:10.1002/er.1105

Yalçın, M. E., Ayhan, T., and Yeniçeri, R. (2020). *Reconfigurable Cellular Neural Networks and Their Applications*, 17840.

Yang, L., Cao, Q., Yu, Y., and Liu, Y. (2020). Comparison of Daily Diffuse Radiation Models in Regions of China without Solar Radiation Measurement. *Energy* 191, 116571. doi:10.1016/j.energy.2019.116571

Yilmaz, A. S., and Özer, Z. (2009). Pitch Angle Control in Wind Turbines above the Rated Wind Speed by Multi-Layer Perceptron and Radial Basis Function Neural Networks. *Expert Syst. Appl.* 36 (6), 9767–9775. doi:10.1016/j.eswa.2009.02.014

Yu, L., Li, Y. P., Huang, G. H., and An, C. J. (2017). A Robust Flexible-Probabilistic Programming Method for Planning Municipal Energy System with

Considering Peak-Electricity price and Electric Vehicle. *Energ. Convers. Manag.* 137, 97–112. doi:10.1016/j.enconman.2017.01.028

Yıldız, B. Y., Şahin, M., Şenkal, O., Pestemalcı, V., and Emrahoğlu, N. (2013). A Comparison of Two Solar Radiation Models Using Artificial Neural Networks and Remote Sensing in turkey. *Energy Sourc. A Recover. Util. Environ. Eff.* 35 (3), 209–217. doi:10.1080/15567036.2011.650276

Zhao, Q., Yao, W., Zhang, C., Wang, X., and Wang, Y. (2019). Study on the Influence of Fog and Haze on Solar Radiation Based on Scattering-Weakening Effect. *Renew. Energ.* 134, 178–185. doi:10.1016/j.renene.2018.11.027

Conflict of Interest: The authors declare that the research was conducted in the absence of any commercial or financial relationships that could be construed as a potential conflict of interest.

Publisher's Note: All claims expressed in this article are solely those of the authors and do not necessarily represent those of their affiliated organizations, or those of the publisher, the editors and the reviewers. Any product that may be evaluated in this article, or claim that may be made by its manufacturer, is not guaranteed or endorsed by the publisher.

APPENDIX 1

TABLE A1 | Linear relationship for best input of 25 cities.

Sites	K_t	TAO	T_{max}	T_{ratio}	ΔT	$T_{Average}$	T_{min}	Alt	Lat	Long	δ	D_{length}	D_{number}	R_h	W_s
Kenitra	6,4645	0,6366	0,0095	0,0475	0,15833	0	0	0	0	0	0	0	0	0	0
Casablanca	5,8901	0,6371	0,0033	0,0165	0,1073	0	0	0	0	0	0	0	0	0	0
Rabat	6,0859	0,6301	0,0076	0,038	0,1267	–3,3404	0	0	0	0	0	0	0	0	0
Safi	4,5053	0,6273	0,0571	0,2855	0,9517	–3,6524	0,007833	–0,0001	32,283	–9,233	–19,98	12,519	0	0	0
Agadir	5,6374	0,6259	0,0518	0,259	0,8633	–3,8515	0	0	0	0	0	0	0	0	0
Essaouira	5,3102	0,6303	0,0671	0,3355	1,11833	0	0	0	0	0	0	0	0	0	0
Settat	6,1852	0,6204	0,3123	1,5615	5,205	–3,3015	0,024733	–0,0045	30,33	–9,41	–8,43	12,524	0	0	0
Dakhla	4,4995	0,6083	-0,021	-0,105	-0,35	–3,8011	–0,03497	–0,0001	23,7	–15,86	–22,08	12,771	0	0	0
El-Aiun	6,3306	0,6337	0,026	0,13	0,4333	–3,8108	0,025333	–0,0076	27,16	–13,21	–20,79	12,695	0	0	0
Sidi Ifni	5,6209	0,6191	0,02	0,1	0,3333	0	0	0	0	0	0	0	0	0	0
Tanger	6,4603	0,6253	0,3142	1,571	5,23667	–3,2704	0,023933	–0,0095	35,733	–5,9	–18,98	12,338	0	0	0
Tetouan	6,0741	0,6257	0,3123	1,5615	5,205	–3,2925	0,020233	–0,0032	35,58	–5,33	–17,45	12,306	0	0	0
Al-Hoceima	5,6909	0,6273	0,0005	0,0025	0	0	0	0	0	0	0	0	0	0	0
Larache	5,1046	0,6221	0,0216	0,108	0	0	0	0	0	0	0	0	0	0	0
Nador	6,0365	0,6245	0,0596	0,298	0,9933	–3,5987	0,013133	–0,0024	35,15	–2,91	–16,23	12,168	0	0	0
Oujda	5,0263	0,6206	0,0554	0,534	2,56387	-4,6523	0,164298	–0,0243	33,75	–1,93	–21,73	11,745	0	0	0
Taza	5,6167	0,604	0,0364	0,182	0,60667	–3,3615	0,010733	–0,0034	34,217	–4	–10,67	12,23	0	0	0
Meknes	5,763	0,621	0,027	0,135	0,663	-4,9640	0,03975	0	0	0	0	0	0	0	0
Beni-Mellal	6,399	0,6082	0,027	0,135	0,45	–3,5805	0,019333	0	0	0	0	0	0	0	0
Ifrane	4,8583	0,6159	0,013	0,065	0,216667	–3,4020	-0,00737	0	0	0	0	0	0	0	0
Fes	6,1079	0,6136	0,3062	1,531	5,103333	–3,0621	0,008933	0	0	0	0	0	0	0	0
Medilt	3,5545	0,6306	0,2583	1,2915	4,305	–28,313	-0,04077	–0,0634	32,683	–4,733	–15,15	12,272	0	0	0
Marrakech	6,5433	0,6351	0,0105	0,0525	0,175	–3,5024	0,015533	–0,0934	31,617	–8,033	–24,66	12,453	0	0	0
Ouarzazate	5,348	0,6241	0,0436	0,218	0	0	0	0	0	0	0	0	0	0	0
Er-Rachidia	6,3443	0,6233	0,0954	0,477	1,59	–4,1873	–0,004	–0,034	31,93	–4,4	–10,45	12,253	0	0	0